

1 **A global water cycle reanalysis (2003–2012) merging**  
2 **satellite gravimetry and altimetry observations with a**  
3 **hydrological multi-model ensemble**

4  
5 **Albert I.J.M. van Dijk<sup>1\*</sup>, Luigi J. Renzullo<sup>2</sup>, Yoshihide Wada<sup>3</sup>, Paul Tregoning<sup>4</sup>**

6  
7 [1] {Fenner School of Environment & Society, The Australian National University, Canberra,  
8 Australia}

9 [2] {CSIRO Land and Water, Canberra, Australia}

10 [3] {Department of Physical Geography, Utrecht University, Utrecht, Netherlands}

11 [4] {Research School of Earth Sciences, The Australian National University, Canberra,  
12 Australia}

13 Correspondence to: Albert Van Dijk, albert.vandijk@anu.edu.au

14  
15 **Abstract**

16 We present a global water cycle reanalysis that reconciles water balance estimates derived  
17 from the GRACE satellite mission, satellite water level altimetry and off-line estimates from  
18 several hydrological models. Error estimates for the sequential data assimilation scheme were  
19 derived from available uncertainty information and the triple collocation technique. Errors in  
20 four GRACE storage products were estimated to be 11–12 mm over land areas, while errors  
21 in monthly storage changes derived from five global hydrological models were estimated to  
22 be 17–28 mm. Prior and posterior estimates were evaluated against independent observations  
23 of river water level and discharge, snow water storage and glacier mass loss. Data  
24 assimilation improved or maintained agreement overall, although results varied regionally.  
25 Uncertainties were greatest in regions where glacier mass loss and sub-surface storage  
26 decline are both plausible but poorly constrained. We calculated a global water budget for  
27 2003–2012. The main changes were a net loss of polar ice caps ( $-342 \text{ Gt y}^{-1}$ ) and mountain  
28 glaciers ( $-230 \text{ Gt y}^{-1}$ ), with an additional decrease in seasonal snow pack ( $-18 \text{ Gt y}^{-1}$ ). Storage  
29 increased due to new impoundments ( $+16 \text{ Gt y}^{-1}$ ), but this was compensated by decreases in

30 other surface water bodies ( $-10 \text{ Gt y}^{-1}$ ). If the effect of groundwater depletion ( $-92 \text{ Gt y}^{-1}$ ) is  
31 excluded, sub-surface water storage increased by  $+110 \text{ Gt y}^{-1}$  due particularly to increased  
32 wetness in northern temperate regions and in the seasonally wet tropics of South America and  
33 southern Africa.

34

## 35 **1. Introduction**

36 More accurate global water balance estimates are needed, to better understand interactions  
37 between the global climate system and water cycle (Sheffield et al., 2012), the causes of  
38 observed sea level rise (Boening et al., 2012; Fasullo et al., 2013; Cazenave et al., 2009;  
39 Leuliette and Miller, 2009), human impacts on water resources (Wada et al., 2010; 2013), and  
40 to improve hydrological models (van Dijk et al., 2011) and initialise water resources forecasts  
41 (Van Dijk et al., 2013). The current generation of global hydrological models have large  
42 uncertainties arising from a combination of data deficiencies (e.g., precipitation in sparsely  
43 gauged regions; poorly known soil, aquifer and vegetation properties) and overly simplistic  
44 descriptions of important water cycle processes (e.g. groundwater dynamics, human water  
45 resources extraction and use, wetland hydrology and glacier dynamics). Data assimilation  
46 (DA) is used routinely to overcome data and model limitations in atmospheric reconstructions  
47 or ‘reanalysis’. In hydrological applications, DA has been largely limited to flood forecasting,  
48 but new applications are being developed (Liu et al., 2012a), including promising  
49 developments towards large-scale water balance reanalyses, alternatively referred to as  
50 monitoring, assessment or estimation (van Dijk and Renzullo, 2011).

51 Here, we undertake a global water cycle reanalysis for the period 2003–2012. Specifically,  
52 we attempt to reconcile global water balance model estimates from different sources with an  
53 ensemble of total water storage (TWS) estimates derived from the Gravity Recovery And  
54 Climate Experiment (GRACE) satellite mission (Tapley et al., 2004). Various alternative  
55 approaches can be conceptualised to achieve this integration and the most appropriate among  
56 these is not obvious. Our approach was to use water balance estimates generated by five  
57 global hydrological models along with several ancillary data sources to generate an ensemble  
58 of prior estimates of monthly water storage changes. Errors in the different model estimates  
59 and GRACE products were estimated spatially through triple collocation (Stoffelen, 1998).  
60 Subsequently, a DA scheme was designed to sequentially reconcile the model ensemble and  
61 GRACE observations. The reanalysis results were evaluated with independent global

62 streamflow records, remote sensing of river water level and snow water equivalent (SWE),  
63 and independent glacier mass balance estimates.

64

## 65 **2. Methods and Data Sources**

### 66 **2.1. Overall approach**

67 We conceptualise TWS ( $S$ , in mm) as the sum of five different water stores ( $s$  in mm), *i.e.*,  
68 water stored in snow and ice ( $s_{snow}$ ); below the surface in soil and groundwater ( $s_{sub}$ ), and in  
69 rivers ( $s_{riv}$ ); lakes ( $s_{lake}$ ), and seas and oceans ( $s_{sea}$ ). We ignore atmospheric water storage  
70 changes, which are removed from the signal during the GRACE TWS retrieval process (e.g.,  
71 Wahr et al., 2006), and vegetation mass changes, which are assumed negligible. The GRACE  
72 TWS estimates are denoted by  $y$  and have the same units as  $S$  but are distinct in their much  
73 smoother spatial character.

74 To date, DA schemes developed for large-scale water cycle analysis typically use Kalman  
75 filter approaches (Liu et al., 2012a). This requires calculation of co-variance matrices and,  
76 presumably because of complexity and computational burden, has only been applied for  
77 single models and limited regions (e.g., Zaitchik et al., 2008). We aimed to develop a DA  
78 scheme that made it possible to use water balance estimates derived ‘off line’ (*i.e.*, in the  
79 absence of DA) so we could use an ensemble of already available model outputs. In the DA  
80 terminology of Bouttier and Courtier (1999), our scheme could be described as sequential and  
81 near-continuous with a spatially variable but temporally stable gain factor. The characteristics  
82 of the DA problem to be addressed in this application were as follows:

83 (1) Alternative GRACE TWS estimates ( $y^o$ ) were available from different processing centres  
84 and error estimates were required for each;

85 (2) Alternative estimates for some of the stores,  $s$ , were available from different hydrological  
86 models with higher definition than  $y^o$ ;

87 (3) Error estimates were required for each store and data source;

88 (4) A method was required to spatially transform between  $s$  and  $y$  as part of the assimilation.

89

## 90        2.2.        Data sources

91        The data used include those needed to derive prior estimates for each of the water cycle  
92        stores, the GRACE retrievals to be assimilated and independent observations to evaluate the  
93        quality of the reanalysis. All are listed in Table 1 and described below.

94        Monthly water balance components from four global land surface model estimates at 1°  
95        resolution were obtained from NASA's Global Data Assimilation System (GLDAS) (Rodell  
96        et al., 2004). The four models include CLM, Mosaic, NOAH and VIC which, for the 2003–  
97        2012, were forced with “a combination of NOAA/GDAS atmospheric analysis fields,  
98        spatially and temporally disaggregated NOAA Climate Prediction Center Merged Analysis of  
99        Precipitation (CMAP) fields, and observation-based radiation fields derived using the method  
100        of the Air Force Weather Agency's AGRicultural METeorological modelling system” (Rui,  
101        2011). The models are described in Rodell et al. (2004). From the model outputs we used (i)  
102        snow water equivalent (SWE) depth, (ii) total soil moisture storage over a soil depth that  
103        varies between models, and (iii) generated streamflow, calculated as the sum of surface  
104        runoff and sub-surface drainage. In addition to GLDAS, we used global water balance  
105        estimates generated by the W3RA model (Van Dijk et al., 2013) in the configuration used in  
106        the Asia-Pacific Water Monitor (<http://eos.csiro.au/apwm/>). For 2003–2008, the model was  
107        forced with the ‘Princeton’ merged precipitation, down-welling short-wave radiation,  
108        minimum and maximum daily temperature and air pressure data produced by Sheffield et al.  
109        (2006). From 2009 onwards, the model primarily uses ‘ERA-Interim’ weather forecast model  
110        reanalysis data from the European Centre for Medium-Range Weather Forecasts. For low  
111        latitudes, these are combined with near-real time TRMM multi-sensor precipitation analysis  
112        data (TMPA 3B42 RT) (Huffman et al., 2007) to improve estimates of convective rainfall  
113        (Peña-Arancibia et al., 2013). Both were bias-corrected with reference to the Princeton data  
114        to ensure homogeneity. W3RA model estimates were conceptually similar to those from  
115        GLDAS, except that the model includes deep soil and groundwater stores and sub-grid  
116        surface and groundwater routing.

117        The five hydrological models do not provide estimates of groundwater depletion and storage  
118        in rivers, lakes and impoundments and these were therefore derived separately. Groundwater  
119        depletion estimates were derived for 1960–2010 by Wada et al. (2012). The time series were  
120        calculated as the net difference between estimated groundwater extraction and recharge.

121        National groundwater extraction data compiled by the International Groundwater Resources  
122        Assessment Centre (IGRAC) were disaggregated using estimates of water use intensity and

123 surface water availability at 0.5° resolution from a hydrological model (PCR-GLOBWB; see  
124 Wada et al., 2012, for details). The model also estimated recharge including return flow from  
125 irrigation. Uncertainty information of groundwater depletion was generated by 10,000 Monte  
126 Carlo simulations, with 100 realizations of extraction and recharge respectively (Wada et al.,  
127 2010). This method tends to overestimate reported depletion in non-arid regions, where  
128 groundwater pumping can enhance recharge from surface water. Wada et al. (2012) used a  
129 universal multiplicative correction to account for this. Here, the correction was calculated per  
130 climate region rather than world-wide, reflecting the dependency of uncertainty on recharge  
131 estimates and their errors. Data for 2011–2012 were not available; these were estimated using  
132 monthly average depletion and uncertainty values for the preceding 2003–2010 period. Given  
133 the regular pattern of depletion in the preceding years this by itself is unlikely to have  
134 affected the analysis noticeably.

135 River water storage was estimated by propagating runoff fields from each of the five models  
136 through a global routing scheme. In a previous study, we compared these runoff fields with  
137 streamflow records from 6,192 small (<10,000 km<sup>2</sup>) catchments worldwide and found that  
138 observed runoff was 1.28 to 1.77 times greater than predicted by the different models (Van  
139 Dijk et al., 2013). The respective values were used to uniformly bias-correct the runoff fields.  
140 Next, we used a global 0.5° resolution flow direction grid (Oki et al., 1999; Oki and Sud,  
141 1998) to parameterise a cell-to-cell river routing scheme. We used a linear reservoir  
142 kinematic wave approximation (Vörösmarty and Moore III, 1991), similar to that used in  
143 several large-scale hydrology models (see recent review by Gong et al., 2011). The monthly  
144 1° runoff fields from each of the five models were oversampled to 0.5° and daily time step  
145 before routing, and the river water storage estimates (in mm) were aggregated back to  
146 monthly 1° grid cell averages before use in assimilation. The routing function was an inverse  
147 linear function of the distance between network nodes and a transfer (or routing) coefficient.  
148 For each model, a globally uniform optimal transfer coefficient was found by testing values  
149 of 0.3 to 0.9 day<sup>-1</sup> in 0.1 day<sup>-1</sup> increments and finding the value that produced best overall  
150 agreement with seasonal flow patterns observed in 586 large rivers world-wide. These 586  
151 were a subset of 925 ocean-reaching rivers for which streamflow records were compiled by  
152 Dai et al. (2009) from various sources; we excluded locations where streamflow records were  
153 available for less than 10 years since 1980 or less than 6 months of the year.

154 The resulting river flow estimates do not account for the impact of river water use (i.e., the  
155 evaporation of water extracted from rivers, mainly for irrigation). We addressed this using

156 global monthly surface water use estimates that were derived in a way similar to that used for  
157 groundwater depletion estimates (details in Wada et al., 2013). For each grid cell, mean water  
158 use rates for 2002–2010 were subtracted from mean runoff estimates for the same period, and  
159 the remaining runoff was routed downstream. The resulting mean net river flow estimates  
160 were divided by the original estimates to derive a scaling factor, which was subsequently  
161 applied at each time step. Lack of additional global information on river hydrology meant  
162 that three simplifications needed to be made: (i) our approach implies that for a particular  
163 grid cell, monthly river water use is assumed proportional to river flow for that month; (ii) the  
164 influence of lakes, wetlands and water storages on downstream flows (e.g., through dam  
165 operation) is not accounted for, even though their actual storage changes are (see further on);  
166 (iii) our approach does not account for losses associated with permanent or ephemeral  
167 wetlands, channel leakage and net evaporation from the river channel. To some extent, the  
168 DA process may correct mass errors resulting from these assumptions.

169 Variations in lake water storage were not modelled, but water level data for 62 lakes world-  
170 wide were obtained from the Crop Explorer web site (Table 1) and include most of the  
171 world's largest lakes and reservoirs, including the Caspian Sea. The water level data for these  
172 lakes were derived from satellite altimetry and converted to mm water storage. Measurements  
173 were typically available every 10 days. The mean and standard deviation for each individual  
174 month were used as best estimate and estimation error, respectively. Storage in water bodies  
175 without altimetry data was necessarily assumed negligible. This includes many small lakes  
176 and dams, but also some larger lakes affected by snow and ice cover (e.g., the Great Bear and  
177 Great Slave Lakes in Canada) and ephemeral, distributed or otherwise complex water bodies  
178 (e.g., the Okavango delta in Botswana and Lake Eyre in Australia, each of which contains  
179  $>10 \text{ km}^3$  of water when full).

180 A list of dams was collated by Lehner et al. (2011) and was updated with large dams  
181 constructed in more recent years with the ICOLD data base (Table 1). For the period 1998–  
182 2012, a total 198 georeferenced dams with a combined storage capacity of  $418 \text{ km}^3$  were  
183 identified. For the Three Gorges Dam ( $39 \text{ km}^3$ ), reservoir water level time series from  
184 <http://www.ctg.com.cn/inc/sqsk.php> were converted to storage volume following Wang et al.  
185 (2011). For the remaining dams, we assumed a gradual increase to storage capacity over the  
186 first five years after construction with a relative estimation error of 20%.

187 Delayed time, up-to-date global merged mean sea level anomalies were obtained from the  
188 Aviso web site (Table 1). The monthly data were reprojected from the native  $1/3^\circ$  Mercator

189 grid to regular 1° grids. An estimate of uncertainty was derived by calculating the spatial  
190 standard deviation in sea level values within a 4° by 4° region around each grid cell during  
191 re-projection. When sea level data were missing, because of sea ice, we assumed sea level did  
192 not change and assigned an uncertainty of 5 mm. Following the recent global sea level budget  
193 study by Chen et al. (2013), we assumed that 75% of the observed sea level change was due  
194 to mass increase, and we multiplied altimetry sea level anomalies with this factor.

195 We did not have spatial global time series of glacier mass changes. The five hydrological  
196 models have an oversimplified representation of ice dynamics, and therefore large  
197 uncertainties and errors can be expected for glaciated regions. To account for this, we used  
198 the ‘GGHYDRO’ global glacier extent mapping by Cogley (2003) to calculate the percentage  
199 glacier area for each grid cell, and assumed a proportional error in monthly glacier mass  
200 change estimates corresponding to 300 mm per unit glacier area. This value was chosen  
201 somewhat arbitrarily and ensures that a substantial fraction of the analysis increment is  
202 assigned to glaciers.

203 Three alternative GRACE TWS retrieval products were downloaded from the Tellus web  
204 site. The three products (coded CSR, JPL and GFZ; release 05) each had 1° (nominal) and  
205 monthly resolution. The land and ocean mass retrievals (Chambers and Bonin, 2012) were  
206 combined. The land retrievals had been ‘de-striped’ and smoothed with a 200 km half-width  
207 spherical Gaussian filter (Swenson et al., 2008; Swenson and Wahr, 2006), whereas the ocean  
208 retrievals had been smoothed with a 500 km filter (Chambers and Bonin, 2012). The DA  
209 method we employed is designed to deal with the signal ‘leakage’ caused by the smoothing  
210 process and therefore we did not use the scaling factors provided by the algorithm  
211 developers. In addition, gravity fields produced by CNES/GRGS (Bruinsma et al., 2010) at 1°  
212 resolution for 10 day periods were used. The three Tellus data sources had been corrected for  
213 Glacial Isostatic Adjustment (GIA); we corrected the GRGS data using the same GIA  
214 estimates of Geruo et al. (2013). Initial DA experiments produced unexpectedly strong mass  
215 trends around the Gulf of Thailand. Inspection demonstrated that all products, to different  
216 degrees, contained a mass redistribution signal associated with the December 2004 Sumatera-  
217 Andaman earthquake. To account for this, we first calculated a time series of seasonally-  
218 adjusted monthly anomalies (i.e., the average seasonal cycle was removed) for the region  
219 [5°N–15°, 80–110°E]. Next, we adjusted values after December 2004 by the difference in the  
220 mean adjusted anomalies for the year before and after the earthquake, respectively.

221

222 **2.3. Data assimilation scheme**

223 For each update cycle, the DA scheme proceeds through the steps illustrated in Figure 1 and  
 224 described below.

225 *1) Deriving the prior estimate for each store.* The way to calculate the prior (or background)  
 226 estimate of storage  $s_t^b$  varied between stores. A systematic and accumulating bias (or ‘drift’)  
 227 was considered plausible for the deep soil and groundwater components of model-derived  
 228 sub-surface storage due to slow groundwater dynamics (including extraction) and ice storage  
 229 in permanent glaciers and ice sheets, which may be progressively melting or accumulating. In  
 230 these cases, the model-estimated *change* in storage was assumed more reliable than the actual  
 231 storage itself, and estimates from the five models were used to calculate storage change,  $\Delta s_t^b$   
 232 for store  $i$  ( $i=1, \dots, N$ ) as:

$$\Delta s_t^b(i) = \sum_{l=1}^L w_l x_t^l(i) \quad (1)$$

233 where  $x_t^l$  is the estimate of storage change from model  $l$  ( $l=1, \dots, L$ ) between time  $t-1$  and  $t$ ,  
 234 and  $w_l$  the relative weight of model  $l$  in the ensemble, computed as:

$$w_l = \frac{\sigma_l^{-2}}{\sum_l \sigma_l^{-2}} \quad (2)$$

235 where  $\sigma_{y,l}^2$  is the error for model  $l$  based on triple collocation (see Section 2.4). Subsequently,  
 236  $s_t^b$  was calculated as:

$$s_t^b(i) = s_{t-1}^{a*}(i) + \Delta s_t^b(i) \quad (3)$$

237 where  $s_{t-1}^{a*}$  is the posterior (or analysis) estimate from the previous time step. This approach  
 238 was not suitable for model-estimated seasonal snowpack and river storage, where the  
 239 ephemeral nature of the storage means that long-term drift is not an issue and Eq. (2) could in  
 240 fact lead to unrealistic negative storage values. For these cases,  $s_t^b$  was computed as:

$$s_t^b(i) = \sum_{l=1}^L w_l s_t^l(i) \quad (4)$$

241 where  $s_t^l$  is the storage estimate from model  $l$ . The glacier extent map was used to identify  
 242 whether Eq. (3) or (4) should be used for  $s_{snow}$ . Similarly, no drift was expected in the ocean  
 243 and lake storage data, and these were used directly as estimates of  $s_t^b$ .



244 2) *Deriving the prior estimate of GRACE-like TWS ( $y^b$ )*. This estimate was derived by  
 245 summing all stores  $s_t^b$  as:

$$S_t^b = \sum_{i=1}^N s_t^b(i) \quad (5)$$

246 and subsequently applying a convolution operator  $\Gamma$  to transform  $S_t^b$  to a ‘GRACE-like’ TWS  
 247  $y^b$ . The operator  $\Gamma$  was a Gaussian smoother (cf. Jekeli, 1981) written here as:

$$y_t^b(j_1) = \sum_{j_1} \Gamma(j_1, j_2) S_t^b(j_1, j_2) \quad (6)$$

248 where  $j_1$  and  $j_2$  in principle should encompass all existing grid cell coordinates. In practice,  $\Gamma$   
 249 was applied as a moving Gaussian kernel with a size of  $6^\circ \times 6^\circ$  and a half-width of 300 km  
 250 (see further on).

251 3) *Updating the GRACE-like TWS*. The updated GRACE-like TWS,  $y_t^a$ , was calculated from  
 252 the prior (Eq. (6)) and GRACE observations  $y_t^o$  for time  $t$  as (cf. Figure 1 a-d):

$$y_t^a = y_t^b + \delta y_t = y_t^b + k(y_t^o - y_t^b) \quad (7)$$

253 where  $\delta y_t$  is the analysis increment and  $k$  a temporally static gain factor derived by  
 254 combining the error variances of modelled and observed  $y$  as follows:

$$k = \frac{\sum_l w_{y,l} \sigma_{y,l}^2}{\sum_l w_{y,l} \sigma_{y,l}^2 + \sum_m w_{y,m} \sigma_{y,m}^2} \quad (8)$$

255 where  $w_{y,l}$  and  $w_{y,m}$  are the weights applied to each of the five GRACE-like TWS estimates  
 256 and four GRACE data sources, respectively, calculated from their respective error variances  
 257  $\sigma_{y,l}^2$  and  $\sigma_{y,m}^2$  analogous to Eq. (2). 4) *Spatially disaggregating the analysis increment to the*  
 258 *different stores*. The observation model was inverted and combined with the store error  
 259 estimates in order to spatially redistribute the analysis increment  $\delta y_t$ , as follows (cf. Figure  
 260 1e-g):

$$\delta s_t(i, j_1) = \sum_{j_2} \Omega(j_1, j_2) \delta y_t(j_2) \quad (9)$$

261 where the redistribution operator  $\Omega$  can be written as (cf. Figure 1g):

$$\Omega(j_1, j_2) = \frac{\Gamma(j_1, j_2) \sigma^{-2}(i, j_2)}{\sum_i \sum_{j_1} \Gamma(j_1, j_2) \sigma^{-2}(i, j_2)} \quad (10)$$

262 To implement this, spatial error estimates are required for each store. For lakes and seas, the  
263 errors were estimated from the observations (see Section 2.2). For the model-based estimates,  
264 the error was calculated for each time step and store as:

$$\sigma_t^2(i) = \sum_l w_l [x_t^l(i) - \Delta s_t^b(i)]^2 \quad (11)$$

265 The resulting error estimates are spatially and temporally dynamic and respond to the  
266 magnitude of the differences between the different model estimates. For  $s_{sub}$  and  $s_{snow}$  we  
267 combined the error estimates derived by Eq. (11) with the estimated errors in groundwater  
268 depletion and glacier mass change, respectively (see Section 2.2), calculating total error as  
269 the quadratic sum of the composite errors.

270 5) *Updating the stores.* In the final step, the state of each store is updated:

$$s_t^a(i) = s_t^b(i) + \delta s_t(i) \quad (12)$$

271 Subsequently, the procedure is repeated for the next time step.

272

## 273 **2.4. Error estimation**

274 Spatial error fields are required for all data sets to calculate the gain factor  $k$  and where  
275 necessary these were estimated using the triple collocation technique (Stoffelen, 1998). This  
276 technique infers errors in three independent time series by analysing the covariance structure.  
277 The approach has been applied widely to estimate errors in, among others, satellite-derived  
278 surface soil moisture (Dorigo et al., 2010; Scipal et al., 2009), evapotranspiration (Miralles et  
279 al., 2011) and vegetation leaf area (Fang et al., 2012). A useful description of the technique,  
280 the assumptions underlying it and an extension of the theory to any number of time series  
281 greater than three was provided by Zwieback et al. (2012). Application requires three (or  
282 more) estimates of the same quantity. This was achieved by convolving the model-derived  
283 storage estimates into large-scale, smoothed TWS estimates equivalent to those derived from  
284 GRACE measurements using Eqs. (5) and (6). Inspection of the original Tellus data made  
285 clear that the 200 km filter that was already applied as part of the land retrieval had only  
286 removed part of the spurious aliasing in the data sets, and propagated these artefacts into the  
287 error estimates and reanalysis. Therefore a smoother, 300 km filter was applied to the Tellus  
288 TWS data sets. Because conceptual consistency is required for triple collocation, the same  
289 filter was applied to the GRGS and model-derived TWS estimates. Several alternative Tellus  
290 and model time series were available, and therefore the triple collocation technique could be

291 used to produce alternative error estimates from multiple triplet combinations (i.e., five for  
292 Tellus TWS, three for model TWS, and  $5 \times 3 = 15$  for GRGS TWS). The agreement between  
293 these alternative estimates was calculated as a measure of uncertainty in estimated errors.

294 Important assumptions of the collocation technique are that: (1) each data set is free of bias  
295 relative to each other, (2) errors do not vary over time, (3) there is no temporal  
296 autocorrelation in the errors, and (4) there is no correlation between the errors in the  
297 respective time series (Zwieback et al., 2012). Each of these assumptions is difficult to  
298 ascertain, but some interpretative points can be made. Errors in the GRACE products vary  
299 somewhat from month to month depending on data availability, and overall decreased after  
300 June 2003. Therefore assumption (2) is a simplification. Assumption (3) is also unlikely to  
301 hold fully: there will almost certainly be systematic errors and biases that cause temporal  
302 correlation in the errors in the modelled TWS (e.g., due to poorly represented processes  
303 causing secular trends such as groundwater extraction or glacier melt). We avoided this  
304 assumption by applying the triple collocation to monthly storage changes rather than actual  
305 storage, although temporal correlation in storage change errors remains a possibility.

306 However, temporal correlation in the GRACE errors is unlikely. Therefore, the error in  
307 individual mass estimates was calculated following conventional error propagation theory, by  
308 dividing the estimated error in mass changes by  $\sqrt{2}$ .

309 Assumption (4) will not be fully met where estimates are partially based on the same  
310 principle or measurement. In this study, arguably the most uncertain assumption is that the  
311 GRGS and Tellus errors are to a large extent uncorrelated. The basis for this assumption is  
312 that most of the error is likely to derive from the TWS retrieval method rather than the  
313 primary measurements (Sakumura et al., 2014). The GRGS time series was selected as the  
314 third triple collocation member because the four Tellus products are retrieved by methods  
315 that are comparatively more similar than the GRGS method, which uses ancillary  
316 observations from the Laser Geodynamics Satellites (Tregoning et al., 2012).

317 Correspondingly, global average correlation among the Tellus TWS time series was stronger  
318 (0.61–0.73) than between any of the Tellus and GRGS time series (0.49–0.58). Nonetheless,  
319 there may well have been a residual covariance between errors in the GRGS and Tellus  
320 products. In triple collocation, this would cause some part of the differences to be wrongly  
321 attributed to the prior estimates rather than the observation products. Therefore, we  
322 conservatively inflated the calculated value by including an additional error of 5 mm through  
323 quadratic summation before calculating the gain factor (Eq. 8).

324 Uncertainty in the derived error estimates also arises from sample size, i.e. the number of  
325 collocated observations ( $N=111$ ). Previous studies have suggested that 100 samples are  
326 sufficient to produce a reasonable estimate (Dorigo et al., 2010), although Zwieback et al.  
327 (2012) calculate that the relative uncertainty in the estimated errors for  $N=111$  can be  
328 expected to be in the order of 20%. Such a modest uncertainty in derived errors will not have  
329 a strong impact on the reanalysis results.

330

## 331 **2.5. Evaluation against observations**

332 Evaluation of the reanalysis results for sub-surface storage was a challenge: ground  
333 observations are not widely available at global scale, are often conceptually not equivalent to  
334 the reanalysis terms, require tenuous scaling assumptions for comparison at  $1^\circ$  grid cell  
335 resolution, and many existing data sets contain few or no records during 2003–2012. For  
336 example, comparison with in situ soil moisture measurements or groundwater bore data is  
337 beset by such problems (Tregoning et al., 2012). Similarly, an initial comparison with near-  
338 surface ( $<5$  cm depth) soil moisture estimates from passive and active microwave remote  
339 sensing (Liu et al., 2012b; Liu et al., 2011) showed that the conceptual difference between the  
340 two quantities was too great for a meaningful comparison.

341 We were able to evaluate the reanalysis for storage in rivers, seasonal snow pack and  
342 glaciers, however. Firstly, a total of 1,264 water level time series for several large rivers  
343 worldwide were obtained from the Laboratoire d'Etudes en Géodésie et Océanographie  
344 Spatiales (LEGOS) HYDROWEB web site (Table 1). The river levels were retrieved from  
345 ENVISAT and JASON-2 satellite altimetry (Crétaux et al., 2011) and included uncertainty  
346 information for each data period. From each time series, we removed data points with an  
347 estimated error of more than 25% of the temporal standard deviation (SD). Another 165  
348 altimetry time series were obtained from the European Space Agency (ESA) River&Lake  
349 web site (Berry, 2009). These were selected to increase measurement period and sample size  
350 for the available locations, as well as extending coverage to additional rivers. The ESA time  
351 series did not include error estimates; instead data plots were judged visually to assess the  
352 likelihood of measurement noise; seemingly affected time series and outlier data points  
353 ( $>3SD$ ) were excluded. The total 1,429 time series were merged for individual  $1^\circ$  grid cells.  
354 In each case, the longest time series was chosen as reference. Overlapping time periods were  
355 used to remove (typically small) systematic biases in water surface elevation between time

356 series; where there was no overlap the time series were normalised by the median water level.  
357 The ESA data were used where or when HYDROWEB data were not available, and merged  
358 time series with fewer than 24 data points in total were excluded. The resulting data set  
359 contained time series for 442 grid cells with an average 61 (maximum 115) data points during  
360 2003–2012. The relationship between river water level and river discharge (i.e., the discharge  
361 rating curve) is usually non-linear but unknown, and therefore a direct comparison could not  
362 be made. Instead, we calculated Spearman’s rank correlation coefficient ( $\rho$ ) between  
363 estimated discharge and observed water level.

364 Secondly, we used the already mentioned discharge data for 586 ocean-reaching rivers world-  
365 wide (Dai et al., 2009). From these, we selected 430 basins for which the reported drainage  
366 area was within 20% of the area derived from the 0.5° routing network. The ratio between  
367 reported and model-derived drainage area was used to adjust the reanalysis estimates and  
368 these were compared with recorded mean streamflow. The recorded mean annual discharge  
369 values are not for 2003–2012, but we assume that the differences are not systematic and,  
370 therefore, that any large change in agreement may still be a useful indicator of reanalysis  
371 quality.

372 Third, snow storage estimates were evaluated with the European Space Agency GlobSnow  
373 product (Luoju et al., 2010). This data set contains monthly 0.25° resolution estimates of  
374 snow water equivalent (SWE, in mm) for low relief regions with seasonal snow cover north  
375 of 55°N during 2003–2011. The SWE estimates are derived through a combination of  
376 AMSR-E passive microwave remote sensing and weather station data (Pulliainen, 2006;  
377 Takala et al., 2009). The GlobSnow data were aggregated to 1° resolution. The root mean  
378 square error (RMSE) and the coefficient of correlation ( $r^2$ ) were calculated as measures of  
379 agreement.

380 Finally, we compared the estimated trends in storage in different glacier regions to trends for  
381 mountain glaciers compiled by Gardner et al. (2013) for 2003–2010 and for Greenland and  
382 Antarctica by Jacob et al. (2012) for 2003–2009. In some cases, these mass balance estimates  
383 were based on independent glaciological or ICESAT satellite observations and these were the  
384 focus of comparison. Other estimates were partially or wholly based on GRACE data, which  
385 makes comparison less insightful.

386

### 387 **3. Results**

### 388        **3.1.        Error estimation**

389        The mean errors derived by the triple collocation technique were of similar magnitude for the  
390        GRACE and model estimates (Table 2; note that the numbers listed are for storage change  
391        rather than storage per se and are not adjusted for GRACE error covariance; cf. Section 2.4).  
392        The relatively low values for the coefficient of variation suggest that the error estimates are  
393        reasonably robust.

394        The spatial error in merged GRACE and model storage change estimates were calculated  
395        analogous to Eq. (8). The resulting GRACE error surface was relatively homogeneous with  
396        an estimated error of around 5–20 mm for most regions, but increasing to 20–40 mm over  
397        parts of the Amazon and the Arctic (Figure 2a). The combined model error surface suggest  
398        that errors are smaller than those in the GRACE data for arid regions (<10 mm) but higher  
399        elsewhere, increasing beyond 80 mm in the Amazon region (Figure 2b). The mean errors  
400        over non-glaciated land areas were similar, at 18.1 mm for the combined model and 13.5 mm  
401        for the combined GRACE data. Assuming no temporal correlation and allowing for error  
402        covariance among GRACE products reduces the latter to 10.8 mm (i.e.,  $\sqrt{13.5^2/2 + 5^2}$ ).

403

### 404        **3.2.        Analysis increments**

405        Inspection of the analysis increments and the overall difference between prior and posterior  
406        estimates provides insights into the functioning of the assimilation scheme (Figure 3). The  
407        spatial pattern in root mean squared (RMS) TWS increments ( $\sqrt{\delta S^2}$ ) emphasises the  
408        important role of the world's largest rivers in explaining mismatches between expected and  
409        observed mass changes, particularly in tropical humid regions (Figure 3a). Large increments  
410        also occurred over Greenland (mainly due to updated ice storage changes) and the seasonally-  
411        wet regions of Brazil, Angola and south Asia (sub-surface storage). When considering the  
412        RMS between prior and posterior estimates of actual TWS as opposed to monthly changes  
413        (Figure 3b) a similar pattern emerges, but with more emphasis on the smaller but  
414        accumulating difference in estimated storage over Greenland, Alaska and part of Antarctica  
415        (due to updated ice mass changes) and northwest India (groundwater depletion).

416

417

### 418        **3.3.        Mass balance and trends**

419 The trend and monthly fluctuations (expressed in standard deviation, SD) in global mean total  
420 water mass provides a test of internal consistency. Among the original GRACE TWS data,  
421 the GRG data showed the smallest temporal SD (0.04 mm) and linear trend ( $0.007 \pm 0.001$   
422 SD mm y<sup>-1</sup>) in global water mass. The three Tellus retrievals showed larger temporal SD  
423 (4.7–6.4 mm) and trends ( $-0.37 \pm 0.21$  to  $-0.23 \pm 0.20$  mm y<sup>-1</sup>). The merged GRACE TWS  
424 data had intermediate SD (3.97 mm) and trend ( $-0.32$  mm y<sup>-1</sup>). Assimilation reduced SD (to  
425 3.1 mm) and removed the residual trend ( $-0.01 \pm 0.10$  mm y<sup>-1</sup>). The discrepancies in global  
426 water mass trends in the merged GRACE data and in the analysis were mostly located over  
427 the oceans, and therefore the achieved mass balance closure can be attributed to the influence  
428 of the prior sea mass change estimates (Figure 4).

429

### 430 **3.4. Regional storage trends**

431 The spatial pattern in linear trends in the merged GRACE TWS ( $y_0$ ) and the synthetic  
432 reanalysis signal ( $y_b$ ) agree well (Figure 4bc), suggesting that the assimilation scheme is able  
433 to reconcile the prior estimates of storage changes and observed storage as intended.  
434 Seasonally adjusted anomalies were calculated for the prior and posterior estimates of the  
435 different water cycle components by subtracting the mean seasonal pattern. The 2003–2012  
436 linear trends in these adjusted anomalies (Figure 5) show that the analysis has (i) increased  
437 spatial variability in sub-surface water storage trends, with amplified increasing and  
438 decreasing trends (Figure 5ab); (ii) drastically changes trends in snow and ice storage and  
439 typically made them more negative (Figure 5cd); (iii) reversed river water storage trends in  
440 the lower Amazon and Congo Rivers (Figure 5ef). The reanalysis shows a complex pattern of  
441 strongly decreasing and increasing sub-surface water storage trends in northwest India  
442 (Figure 5b). This may be an artefact from incorrectly specified errors in the groundwater  
443 depletion estimates (see Section 4.2). Less visible is that the analysis often reduced negative  
444 storage trends in other regions with groundwater depletion, that is, decreased the magnitude  
445 of estimated depletion. Because all sub-surface storage terms were combined, a revised  
446 estimate of groundwater depletion cannot be calculated directly, but it can be estimated: for all  
447 grid cells with significant prior groundwater depletion estimates ( $>0.5$  mm y<sup>-1</sup>, representing  
448 99% of total global groundwater depletion) the 2003–2012 trend in sub-surface storage  
449 change was estimated a priori at  $-168 \pm 3$  (SD) km<sup>3</sup> y<sup>-1</sup> of which 157 km<sup>3</sup> (94%) due to  
450 groundwater depletion and the remaining -11 km<sup>3</sup> due to climate variability. Analysis

451 reduced the total trend for these grid cells to  $-103 \pm 3 \text{ km}^3$  per year, from which a revised  
452 groundwater extraction estimate of ca.  $92 \text{ km}^3$  can be derived.  
453 From the seasonally adjusted anomalies, time series and trends of global storage in different  
454 water cycle components were calculated. We calculated snow and ice mass change separately  
455 for regions with seasonal snow cover, high ( $>55^\circ$ ) latitude glaciers, and remaining glaciers  
456 (Figure 6). The mean 2003–2012 trends are listed in Table 3; for the posterior estimates also  
457 as equivalent sea level rise (SLR, by dividing by the fraction of Earth’s surface occupied by  
458 oceans, i.e., 0.7116) and volume ( $\text{km}^3 \text{ y}^{-1}$ , equivalent to  $\text{Gt y}^{-1}$ ). Some of the effects of the  
459 assimilation were to (i) remove the decreasing trend in prior global terrestrial sub-surface  
460 water storage estimates (Figure 6a), (ii) change the poor prior estimates of polar ice cap mass  
461 considerably (Figure 6fg), (iii) reduce the estimated rate of ocean mass increase from  $1.84 \pm$   
462  $0.06$  (SD) mm to  $1.45 \pm 0.05$  mm (Table 3), and (iv) achieve mass balance closure between net  
463 terrestrial and ocean storage changes (cf. Section 3.3).

464

### 465 **3.5. Evaluation against river level remote sensing**

466 The rank correlation ( $\rho$ ) between river water level and estimated discharge for the 445 grid  
467 cells with altimetry time series are shown in Figure 7. Overall there was no significant change  
468 in agreement between the prior ( $\rho = 0.63 \pm 0.27$  SD) and posterior ( $\rho = 0.63 \pm 0.26$ )  
469 estimates, with an average change of  $+0.01 \pm 0.12$ . However,  $\rho$  did improve for more  
470 locations than it deteriorated (286 vs. 159). There are some spatial patterns in the influence of  
471 assimilation (Figure 7c): strong improvements in the northern Amazon and Orinoco basins  
472 and most African rivers, except for some stations along the Congo and middle Nile Rivers,  
473 and reduced agreement for rivers in China (where prior estimates agreed well) and most  
474 stations in the Paraná and Uruguay basins (where they did not). In most remaining rivers,  
475 agreement did not change much; in some cases because it was already very good (e.g., the  
476 Ganges-Brahmaputra and remainder of the Amazon basin). Altimetry and estimated  
477 discharge time series are shown in Figure 8 for grid cells with the most data points in three  
478 large river systems. In these cases, there is reasonably clear improvement in agreement.

479

### 480 **3.6. Evaluation against historic river discharge observations**

481 The prior estimate of discharge (i.e., the error-weighted average of the four bias-corrected  
482 models) provided estimates that were already considerably better than any of the individual  
483 members (Table 4, Figure 9). Assimilation led to small improvements in RMSE, from 47 to



484 44 km<sup>3</sup> y<sup>-1</sup>, and a very slight increase in the median absolute percentage difference, from 40  
485 to 41%. Combined recorded discharge from the 430 selected basins was 20,909 km<sup>3</sup> y<sup>-1</sup>,  
486 representing 90% of estimated total discharge to the world's oceans according to Dai et al.  
487 (2009). Assimilation improved the agreement with this number from -11% to -4%, of which  
488 about half (5%) is due to a closer estimate of Amazon River discharge. However, modelled  
489 and observed discharge values relate to different time periods and so it is not clear whether  
490 this should be considered evidence for improvement or merely reflects multi-annual  
491 variability.

492

### 493 **3.7. Evaluation against snow water equivalent remote sensing**

494 The spatial RMSE and correlation between the prior and posterior snow water equivalent  
495 (SWE) estimates and the GlobSnow retrievals are shown in Figure 10. Although RMSE  
496 deteriorated in a majority (57%) of grid cells, correlation remained unchanged at  $R^2=0.79$  and  
497 average RMSE improved slightly from 23.2 to 22.3 mm. Assimilation appeared most  
498 successful for grid cells with large prior RMSE in northern Canada (Figure 10a-c).

499

### 500 **3.8. Evaluation against glacier mass balance estimates**

501 Glacier mass changes reported in literature (Gardner et al., 2013; Jacob et al., 2012) are listed  
502 in Table 5 and compared to regional mass trends associated with glaciers and other  
503 components of the terrestrial water derived from the analysis. In the polar regions (e.g.,  
504 Antarctica, Greenland, Iceland, Svalbard, and the Russian Arctic) a large part of the gravity  
505 signal is necessarily from glacier mass change. Published trends for most of these regions  
506 also heavily rely on GRACE data and hence our estimates are generally in good agreement.  
507 Remaining differences can be attributed to the products, product versions and post-processing  
508 methods used, without providing insight into the accuracy of our analysis estimates. In the  
509 other regions, the glaciated areas are smaller and surrounded by ice-free terrain, which  
510 strongly increases the potential for incorrect distribution of analysis increments, as evidenced  
511 by the high trend ratios (>47%, last column Table 5). As a consequence, glacier mass trends  
512 are not well constrained by GRACE data alone and alternative observations are required. The  
513 agreement with independently derived trend estimates varies. For the Canadian Arctic  
514 Archipelago, Alaska and adjoining North America, the assimilation scheme assigns only 55%  
515 (68 Gt y<sup>-1</sup>) of the total regional negative mass trend (-124 Gt y<sup>-1</sup>) to glacier mass changes,  
516 with most of the remainder (40% or 50 Gt y<sup>-1</sup>) assigned to sub-surface water storage changes.

517 Excluding regions for which independent storage change estimates are not available  
518 (Greenland, Antarctica and Patagonia), our estimate of total glacier storage change in the  
519 world's glaciers ( $-114 \text{ km}^3 \text{ y}^{-1}$ ) was  $101 \text{ km}^3 \text{ y}^{-1}$  less than the estimate of *Gardner et al.*  
520 (2013) ( $-215 \text{ km}^3 \text{ y}^{-1}$ ).

521

## 522 **4. Discussion**

### 523 **4.1. Estimated errors**

524 The triple collocation method produced estimates of errors in month-to-month changes in  
525 GRACE TWS estimates of 12.8–14.3 mm over non-glaciated land areas. From these,  
526 GRACE TWS errors of 10.4–12.0 mm can be estimated (cf. Section 3.1). By comparison,  
527 reported uncertainty estimates based on formal error propagation are larger, usually in the  
528 order of 20–25 mm (e.g., Landerer and Swenson, 2012; Tregoning et al., 2012; Wahr et al.,  
529 2006). One plausible explanation is that the 5 mm we assumed to correct for potential  
530 covariance in errors between the GRACE products is too low, another that the formal  
531 uncertainty estimates are too conservative. Inflating the GRACE error estimates by 10 mm  
532 instead of 5 mm reduced the gain by 18% on average. The resulting uncertainty in the  
533 analysis is modest (see next section). Formal error analyses predict that the retrieval errors  
534 decrease towards the poles due to the closer spacing of satellite overpasses (Wahr et al.,  
535 2006), but surprisingly we did not find such a latitudinal pattern.

536 The mean errors in monthly changes in prior TWS for the different models were 16.5–27.9  
537 mm. We do not have independent estimates of errors in modelled large-scale TWS with  
538 which to compare, but the estimates would seem plausible and perhaps less than we  
539 anticipated. From a theoretical perspective, violation of the assumptions underpinning triple  
540 collocation is likely to have produced overestimates of model error, if anything. The  
541 calculated error in the prior estimates over oceans and very stable regions such as Mongolia  
542 and the Sahara are around 5 mm (Figure 2). This provides some further evidence to suggest  
543 that the 5 mm GRACE error inflation we applied may have been reasonable. The largest  
544 errors in the merged model estimates ( $>40 \text{ mm}$ ) were found for humid tropical regions and  
545 high latitudes. The former may be attributed to the combination of large storage variations  
546 and often uncertain rainfall estimates. Precipitation measurements are also fewer at high  
547 latitudes, and here the poor prediction of snow and ice dynamics and melt water river  
548 hydrology are also important factors.

549

## 550 **4.2. Assimilation scheme performance**

551 The spatial pattern in analysis increments emphasises the importance of water stores other  
552 than the soil in explaining discrepancies between model and GRACE TWS estimates (Figure  
553 3). Adjustments to storage changes in large rivers, groundwater depletion, mass changes in  
554 high latitude ice caps and glaciers (e.g., Greenland, Alaska and Antarctica) and lake water  
555 levels (e.g., the Caspian Sea and the North-American Great Lakes) were all considerable  
556 within their region, absorbing monthly analysis increments or long-term trend discrepancies  
557 or both.

558 Uncertainty in error estimates for the different data sources affects the analysis in different  
559 ways. Incorrect estimation of GRACE and model-derived TWS errors by the triple  
560 collocation method primarily affects (i) the weighting of the ensemble members and (ii) the  
561 gain matrix. Appropriate weighting only requires that the relative magnitude of errors among  
562 ensemble members is estimated correctly (cf. Eq. (2)). The average errors for the different  
563 GRACE TWS estimates were all within 14% of the ensemble average (Table 2) and did not  
564 have strong spatial patterns, and therefore the analysis would likely have been very similar if  
565 equal weighting had been applied (cf. Sakumura et al., 2014). Estimated model errors showed  
566 greater differences (up to 52% greater than the ensemble mean, Table 2) as well as regional  
567 patterns. However, the relative rankings and their spatial pattern were robust to the choice of  
568 GRACE TWS members in triple collocation, as evidenced by a low coefficient of variation  
569 (Table 2). This suggests that the errors were correctly specified in a relative sense. For the  
570 gain matrix, the relative magnitude of errors in GRACE *versus* model TWS ensemble means  
571 needed to be estimated correctly (cf. Eq. (8)). The estimated GRACE TWS ensemble errors  
572 are reasonably homogeneous in space (Figure 1a) which increases our confidence in their  
573 validity. The uncertainty due to the correction for assumed correlation between the GRGS  
574 and Tellus TWS (see previous section) is further mitigated by the design of the DA scheme:  
575 the gain factor determines how rapidly the analysis converges towards the GRACE  
576 observations and therefore is important for month-to-month variations, but long-term trends  
577 in TWS will still approach those in the GRACE observations (cf. Figure 4b and c).

578 The main sources of uncertainty in long-term trends in the individual water balance terms are  
579 (i) the removal of non-hydrological mass trends in the GRACE TWS time series and (ii)  
580 accurate specification of relative errors in the individual water balance terms, which is needed  
581 for correct redistribution of the integrated TWS analysis increments. For example, the

582 analysis results illustrate the insufficiently constrained problem of separating gravity signals  
583 due to mass changes in mountain glaciers from nearby sub-surface water storage changes.  
584 This was particularly evident around the Gulf of Alaska and northwest India, where decreases  
585 can be expected not only in glacier mass but also in sub-surface storage due to, respectively, a  
586 regional drying trend and high groundwater extraction rates (Figure 5a). We suspect that  
587 unexpectedly strong increasing storage trends in parts of northwest India are because the  
588 prior groundwater depletion estimates were too high and the assigned errors too low, causing  
589 the analysis update to distribute increments incorrectly. We could have addressed this by  
590 inflating the local groundwater depletion estimation errors, but more research is needed to  
591 understand the underlying causes. Plausible causes are that groundwater extraction is  
592 overestimated, or that extraction is compensated by induced groundwater recharge (e.g., from  
593 connected rivers) (see Wada et al., 2010 for further discussion).

594 Mass balance closure was not enforced and hence provides a useful diagnostic of reanalysis  
595 quality. The GRGS product achieved approximate global mass balance closure at all time  
596 scales, but the three Tellus products showed a seasonal cycle and long-term negative trend in  
597 global water mass. Accounting for atmospheric water vapour mass changes (from ERA-  
598 Interim reanalysis and the NVAP-M satellite product, data not shown) could not explain the  
599 trends and in fact increased the seasonal cycle in global water mass. Data assimilation  
600 reduced the seasonal cycle and entirely removed the trend in total water mass, thanks to the  
601 prior estimates of sea mass increase. For comparison, we calculated average ocean mass  
602 increases by an alternative, more conventional method, which involved avoiding areas likely  
603 to be affected by nearby land water storage changes. Excluding a 1000 km buffer zone  
604 produced a 2003–2012 mass trend of +0.58 to +0.72 mm y<sup>-1</sup> for the three Tellus retrievals,  
605 +1.12 mm y<sup>-1</sup> for the GRGS retrieval, and +0.75 mm y<sup>-1</sup> for the merged GRACE data. Data  
606 assimilation produced a stronger trend of +1.22 mm y<sup>-1</sup> due to the influence of the prior  
607 estimate of +1.67 mm y<sup>-1</sup>. Our prior estimate followed Chen et al. (2013), who used an  
608 iterative modelling approach to attribute 75% of altimetry-observed SLR to mass increase.  
609 Chen et al. (2013) argue that the conventional method produces underestimates of ocean mass  
610 increase. Indeed, the trends we calculated for the ‘buffered’ ocean regions are lower than for  
611 the entire oceans (+1.22 vs. +1.45 mm y<sup>-1</sup> for the reanalysis, and +1.67 vs. +1.84 mm y<sup>-1</sup> for  
612 the prior estimates; Table 3). However the reduction in sea mass change of 0.39 mm y<sup>-1</sup> from  
613 prior to analysis is likely to reopen the problem of reconciling mass and temperature

614 observations with the altimetry derived mean sea level rise of  $+2.45 \pm 0.08 \text{ mm y}^{-1}$  (cf. Chen  
615 et al., 2013).

616

### 617 **4.3. Evaluation against observations**

618 The reanalysis generally did not have much impact on the agreement with river and snow  
619 storage observations, with small improvements for some locations and small degradations for  
620 others. While a robust increase in the agreement would have been desirable, the fact that  
621 agreement was not degraded overall was encouraging. The data assimilation procedure  
622 applied has the important benefit of bringing the estimates into agreement with GRACE  
623 observations. Moreover, performance improvements with respect to river discharge and level  
624 data did occur in the Amazon, where they make an important contribution to TWS changes.  
625 Similarly, snow water equivalent estimates were improved in the North-American Arctic,  
626 where errors in the prior estimates were largest. This demonstrates that GRACE data can  
627 indeed be successfully used to constrain water balance estimates, although further  
628 development may be needed to avoid some of the undesired performance degradation for  
629 water balance components that do not contribute much to the TWS signal.

630 The models used for our prior estimates provided poorly constrained estimates of ice mass  
631 balance changes, and our reanalysis ice mass loss estimates should not be assumed more  
632 accurate than estimates based on more direct methods (Table 5). Our analysis is unique when  
633 compared to previous estimates based on GRACE, in that data assimilation allowed some of  
634 the observed mass changes to be attributed to other water balance components within the  
635 same region, depending on relative uncertainties in the prior estimates. Comparison against  
636 independent estimates of glacier mass balance changes also demonstrated the challenge of  
637 correct attribution, however. Glacier mass balance estimates were in good agreement for  
638 several regions, but estimates for North American glaciers in particular were questionable:  
639 their combined mass loss ( $-68 \text{ Gt y}^{-1}$ ) was much lower than the estimates derived by  
640 independent means ( $-124 \text{ Gt y}^{-1}$ ; Table 5). This can be explained by incorrect specification of  
641 errors. Two caveats are made: (i) the GIA signal is relatively large for these three regions  
642 ( $+50 \text{ Gt y}^{-1}$ ) and hence GIA estimation errors may have had an impact; and (ii) a significant  
643 change in sub-surface water storage is plausible in principle; for example, higher summer  
644 temperatures could be expected to enhance permafrost melting and runoff, as well as enhance  
645 evaporation. More accurate spatiotemporal observation and modelling of glacier dynamics  
646 would appear to be necessary to resolve this issue.

647

#### 648 **4.4. Contributions to sea level rise**

649 The reanalysis estimate of net terrestrial water storage change of  $-495 \text{ Gt y}^{-1}$  (Table 3)  
650 appears a plausible estimate of ocean mass change, equivalent to ca.  $+1.4 \text{ mm y}^{-1}$  sea level  
651 rise. Our results confirmed that mass loss from the polar ice caps is the greatest contributor to  
652 net terrestrial water loss, with Antarctica and Greenland together contributing  $-342 \text{ Gt y}^{-1}$ .  
653 The next largest contribution was from the remaining glaciers. We combine the reanalysis  
654 estimate of  $-129 \text{ Gt y}^{-1}$  with another  $-101 \text{ Gt y}^{-1}$  estimated to be misattributed (cf. Section 3.8)  
655 and obtain a revised estimate of  $-230 \text{ Gt y}^{-1}$ . A small but significant contribution of  $-18 \text{ Gt y}^{-1}$   
656 (Table 3) was estimated to originate from reductions in seasonal snow cover (particularly in  
657 Quebec and Siberia; Figure 5cd). Inter-annual changes in river water storage were not  
658 significant. Small contributions of  $-10 \text{ Gt y}^{-1}$  and  $+16 \text{ Gt y}^{-1}$  were attributed to storage  
659 changes in existing lakes and large new dams, respectively, and compensated each other. The  
660 largest change in an individual water body was in the Caspian Sea ( $-27 \text{ Gt y}^{-1}$ , cf. Figure 5)  
661 which experiences strong multi-annual water storage variations depending on Volga River  
662 inflows.

663 Finally, the analysis suggested a statistically insignificant change of  $+9 \text{ Gt y}^{-1}$  in sub-surface  
664 storage globally. Adding back the suspected misattribution of  $101 \text{ Gt y}^{-1}$  associated with  
665 glaciers produces a revised estimate of  $+110 \text{ Gt y}^{-1}$  (cf. Figure 6a). Combining this with the  
666  $-92 \text{ Gt y}^{-1}$  attributed to groundwater depletion suggests that storage over the remaining land  
667 areas increased by  $202 \text{ Gt y}^{-1}$ . Calculating sub-surface storage trends by latitude band  
668 suggests that most of the terrestrial water ‘sink’ can be found north of  $40^\circ\text{N}$  and between  $0^\circ$ –  
669  $30^\circ\text{S}$  and is opposite to the prior estimates (Figure 11). The main tropical regions  
670 experiencing increases are in the Okavango and upper Zambezi basins in southern Africa and  
671 the Amazon and Orinoco basins in northern South America (Figure 5b). Storage increases for  
672 these regions are also evident from the original GRACE data (Figure 4a) and cannot be  
673 attributed to storage changes in rivers or large lakes. The affected regions contain low relief,  
674 poorly drained areas with (seasonally) high rainfall. In such environments, the storage  
675 changes could occur in the soil, groundwater, wetlands, or a combination of these. Further  
676 attribution is impossible without additional constraining observations (Tregoning et al., 2012;  
677 van Dijk et al., 2011). The ten-year analysis period is short and this cautions against over-  
678 interpreting this apparent ‘tropical water sink’. However it is of interest to note that a gradual  
679 strengthening of global monsoon rainfall extent and intensity has been observed, and is

680 predicted to continue (Hsu et al., 2012). In any event, the difference between prior and  
681 posterior trends in Figure 11 illustrates that the current generation hydrological models, even  
682 as an ensemble, should not be assumed a reliable surrogate observation of long-term sub-  
683 surface groundwater storage changes. GRACE observations proved valuable in improving  
684 these estimates.

685

## 686 **5. Conclusions**

687 We presented a global water cycle reanalysis that reconciles four total water storage retrieval  
688 products derived from GRACE observations with water balance estimates derived from an  
689 ensemble of five global hydrological models, water level measurements from satellite  
690 altimetry, and ancillary data. We summarise our main findings as follows:

- 691 1. The data assimilation scheme generally behaves as desired, but in hydrologically complex  
692 regions the analysis can be affected by poorly constrained prior estimates and error  
693 specification. The greatest uncertainties occur in regions where glacier mass loss and sub-  
694 surface storage declines (may) both occur but are poorly known (e.g., northern India and  
695 North-American glaciers).
- 696 2. The error in original GRACE TWS data was estimated to be around 11–12 mm over non-  
697 glaciated land areas. Errors in the prior estimates of TWS changes are estimated to be 17–  
698 28 mm for the five models.
- 699 3. Water storage changes in other water cycle components (seasonal snow, ice, lakes and  
700 rivers) are often at least as important and uncertain as changes as sub-surface water  
701 storage in reconciling the various information sources.
- 702 4. The analysis results were compared to independent river water level measurements by  
703 satellite altimetry, river discharge records, remotely sensed snow water storage, and  
704 independent estimates of glacier mass loss. In all cases the agreement improved or  
705 remained stable compared to the prior estimates, although results varied regionally. Better  
706 estimates and error specification of groundwater depletion and mountain glacier mass loss  
707 are required.
- 708 5. Data assimilation achieved mass balance closure over the 2003–2012 period and  
709 suggested an ocean mass increase of ca.  $1.45 \text{ mm y}^{-1}$ . This reopens some question about  
710 the reasons for an apparently unexplained  $0.39 \text{ mm y}^{-1}$  (16%) of  $2.45 \text{ mm y}^{-1}$  satellite  
711 observed sea level rise for the analysis period (Chen et al., 2013).

712 6. For the period 2003–2012, we estimate glaciers and polar ice caps to have lost around 572  
713 Gt  $y^{-1}$ , with an additional small contribution from seasonal snow ( $-18 \text{ Gt } y^{-1}$ ). The net  
714 change in surface water storage in large lakes and rivers was insignificant, with  
715 compensating effects from new reservoir impoundments ( $+16 \text{ Gt } y^{-1}$ ), lowering water  
716 level in the Caspian Sea ( $-27 \text{ Gt } y^{-1}$ ) and increases in the other lakes combined ( $+16 \text{ Gt } y^{-1}$ ).  
717 The net change in subsurface storage was significant when considering a likely  
718 misattribution of glacier mass loss, and may be as high as  $+202 \text{ Gt } y^{-1}$  when excluding  
719 groundwater depletion ( $-92 \text{ Gt } y^{-1}$ ). Increases were mainly in northern temperate regions  
720 and in the seasonally wet tropics of South America and southern Africa ( $+87 \text{ Gt } y^{-1}$ ).  
721 Continued observation will help determine if these trends are due to transient climate  
722 variability or likely to persist.

723

## 724 **Acknowledgements**

725 GRACE land data were processed by Sean Swenson and the ocean data by Don P. Chambers,  
726 both supported by the NASA MEASURES Program, and are available at  
727 <http://grace.jpl.nasa.gov>. The GLDAS and TMPA data used in this study were acquired as  
728 part of the mission of NASA's Earth Science Division and archived and distributed by the  
729 Goddard Earth Sciences (GES) Data and Information Services Center (DISC). Lake and  
730 reservoir surface height variations were from the USDA's Global Reservoir and Lake  
731 (GRLM) web site [/www.pecad.fas.usda.gov/cropexplorer/global\\_reservoir/](http://www.pecad.fas.usda.gov/cropexplorer/global_reservoir/), funded by  
732 USDA/FAS/OGA and NASA Global Agriculture Monitoring (GLAM) Project. Altimetric  
733 lake level time-series variations were from the Topex/Poseidon, Jason-1, Jason-2/OSTM, and  
734 Geosat Follow-On (GFO) missions.

735

## 736 **References**

737 Boening, C., Willis, J. K., Landerer, F. W., Nerem, R. S., and Fasullo, J.: The 2011 La Niña:  
738 So strong, the oceans fell, *Geophysical Research Letters*, 39, L19602,  
739 10.1029/2012gl053055, 2012.

740 Bouttier, F., and Courtier, P.: Data assimilation concepts and methods, ECMWF  
741 Meteorological Training Course Lecture Series, 14, 1999.



742 Bruinsma, S., Lemoine, J.-M., Biancale, R., and Valès, N.: CNES/GRGS 10-day gravity field  
743 models (release 2) and their evaluation, *Advances in Space Research*, 45, 587-601, doi:  
744 10.1016/j.asr.2009.10.012, 2010.

745 Cazenave, A., Dominh, K., Guinehut, S., Berthier, E., Llovel, W., Ramillien, G., Ablain, M.,  
746 and Larnicol, G.: Sea level budget over 2003-2008: A reevaluation from GRACE space  
747 gravimetry, satellite altimetry and Argo, *Global and Planetary Change*, 65, 83-88, 2009.

748 Chambers, D. P., and Bonin, J. A.: Evaluation of Release-05 GRACE time-variable gravity  
749 coefficients over the ocean, *Ocean Sci.*, 8, 859-868, 10.5194/os-8-859-2012, 2012.

750 Chen, J. L., Wilson, C. R., and Tapley, B. D.: Contribution of ice sheet and mountain glacier  
751 melt to recent sea level rise, *Nature Geosci*, 6, 549-552, 10.1038/ngeo1829, 2013.

752 Cogley, J. G.: GGHYDRO-Global Hydrographic Data, release 2.3, Technical Note 2003-1,  
753 Dept. of Geographty, Trent University, Peterborough, Ontario, Canada, 2003.

754 Crétaux, J. F., Jelinski, W., Calmant, S., Kouraev, A., Vuglinski, V., Bergé-Nguyen, M.,  
755 Gennero, M. C., Nino, F., Abarca Del Rio, R., Cazenave, A., and Maisongrande, P.: SOLS: A  
756 lake database to monitor in the Near Real Time water level and storage variations from  
757 remote sensing data, *Advances in Space Research*, 47, 1497-1507, doi:  
758 10.1016/j.asr.2011.01.004, 2011.

759 Dai, A., Qian, T., Trenberth, K. E., and Milliman, J. D.: Changes in continental freshwater  
760 discharge from 1948 to 2004, *Journal of Climate*, 22, 2773-2792, 2009.

761 Dorigo, W. A., Scipal, K., Parinussa, R. M., Liu, Y. Y., Wagner, W., De Jeu, R. A. M., and  
762 Naeimi, V.: Error characterisation of global active and passive microwave soil moisture  
763 datasets, *Hydrol. Earth Syst. Sci*, 14, 2605-2616, 2010.

764 Fang, H., Wei, S., Jiang, C., and Scipal, K.: Theoretical uncertainty analysis of global  
765 MODIS, CYCLOPES, and GLOBCARBON LAI products using a triple collocation method,  
766 *Remote Sensing of Environment*, 124, 610-621, doi: 10.1016/j.rse.2012.06.013, 2012.

767 Fasullo, J. T., Boening, C., Landerer, F. W., and Nerem, R. S.: Australia's unique influence  
768 on global sea level in 2010–2011, *Geophysical Research Letters*, 40, 4368-4373,  
769 10.1002/grl.50834, 2013.

770 Gardner, A. S., Moholdt, G., Cogley, J. G., Wouters, B., Arendt, A. A., Wahr, J., Berthier, E.,  
771 Hock, R., Pfeffer, W. T., Kaser, G., Ligtenberg, S. R. M., Bolch, T., Sharp, M. J., Hagen, J.

772 O., van den Broeke, M. R., and Paul, F.: A Reconciled Estimate of Glacier Contributions to  
773 Sea Level Rise: 2003 to 2009, *Science*, 340, 852-857, 10.1126/science.1234532, 2013.

774 Geruo, A., Wahr, J., and Zhong, S.: Computations of the viscoelastic response of a 3-D  
775 compressible Earth to surface loading: an application to Glacial Isostatic Adjustment in  
776 Antarctica and Canada, *Geophysical Journal International*, 192, 557-572, 2013.

777 Gong, L., Halldin, S., and Xu, C. Y.: Global-scale river routing—an efficient time-delay  
778 algorithm based on HydroSHEDS high-resolution hydrography, *Hydrological Processes*, 25,  
779 1114-1128, 10.1002/hyp.7795, 2011.

780 Hsu, P.-c., Li, T., Luo, J.-J., Murakami, H., Kitoh, A., and Zhao, M.: Increase of global  
781 monsoon area and precipitation under global warming: A robust signal?, *Geophysical  
782 Research Letters*, 39, L06701, 10.1029/2012GL051037, 2012.

783 Huffman, G. J., Adler, R. F., Bolvin, D. T., Gu, G. J., Nelkin, E. J., Bowman, K. P., Hong,  
784 Y., Stocker, E. F., and Wolff, D. B.: The TRMM multisatellite precipitation analysis  
785 (TMPA): Quasi-global, multiyear, combined-sensor precipitation estimates at fine scales,  
786 *Journal of Hydrometeorology*, 8, 38-55, 2007.

787 Jacob, T., Wahr, J., Pfeffer, W. T., and Swenson, S.: Recent contributions of glaciers and ice  
788 caps to sea level rise, *Nature*, 482, 514-518, 2012.

789 Jekeli, C.: *Alternative Methods to Smooth the Earth's Gravity Field*. Report 327, Dep. of  
790 Geod. Sci. and Surv., Ohio State Univ., Columbus, Ohio, 1981.

791 Landerer, F. W., and Swenson, S. C.: Accuracy of scaled GRACE terrestrial water storage  
792 estimates, *Water Resources Research*, 48, W04531, 10.1029/2011WR011453, 2012.

793 Lehner, B., Liermann, C. R., Revenga, C., Vörösmarty, C., Fekete, B., Crouzet, P., Döll, P.,  
794 Endejan, M., Frenken, K., Magome, J., Nilsson, C., Robertson, J. C., Rödel, R., Sindorf, N.,  
795 and Wissler, D.: High-resolution mapping of the w'rd's reservoirs and dams for sustainable  
796 river-flow management, *Frontiers in Ecology and the Environment*, 9, 494-502,  
797 10.1890/100125, 2011.

798 Leuliette, E. W., and Miller, L.: Closing the sea level rise budget with altimetry, Argo, and  
799 GRACE, *Geophys. Res. Lett.*, 36, L04608, 10.1029/2008gl036010, 2009.

800 Liu, Weerts, A. H., Clark, M., Hendricks Franssen, H. J., Kumar, S., Moradkhani, H., Seo, D.  
801 J., Schwanenberg, D., Smith, P., van Dijk, A. I. J. M., van Velzen, N., He, M., Lee, H., Noh,  
802 S. J., Rakovec, O., and Restrepo, P.: Advancing data assimilation in operational hydrologic

803 forecasting: progresses, challenges, and emerging opportunities, *Hydrol. Earth Syst. Sci.*, 16,  
804 3863-3887, 10.5194/hess-16-3863-2012, 2012a.

805 Liu, Y. Y., Parinussa, R. M., Dorigo, W. A., De Jeu, R. A. M., Wagner, W., van Dijk, A.,  
806 McCabe, M. F., and Evans, J. P.: Developing an improved soil moisture dataset by blending  
807 passive and active microwave satellite-based retrievals, *Hydrol. Earth Syst. Sci.*, 15, 425-436,  
808 2011.

809 Liu, Y. Y., Dorigo, W., Parinussa, R., De Jeu, R., Wagner, W., McCabe, M., Evans, J., and  
810 Van Dijk, A.: Trend-preserving blending of passive and active microwave soil moisture  
811 retrievals, *Remote Sensing of Environment*, 123, 280-297, 2012b.

812 Luojus, K., Pulliainen, J., Takala, M., Derksen, C., Rott, H., Nagler, T., Solberg, R.,  
813 Wiesmann, A., Metsamaki, S., Malnes, E., and Bojkov, B.: Investigating the feasibility of the  
814 globsnow snow water equivalent data for climate research purposes, *Geoscience and Remote  
815 Sensing Symposium (IGARSS), 2010 IEEE International*, 2010,

816 Miralles, D. G., De Jeu, R. A. M., Gash, J. H., Holmes, T. R. H., and Dolman, A. J.:  
817 Magnitude and variability of land evaporation and its components at the global scale, *Hydrol.  
818 Earth Syst. Sci.*, 15, 967-981, 10.5194/hess-15-967-2011, 2011.

819 Oki, T., and Sud, Y. C.: Design of Total Runoff Integrating Pathways (TRIP)-A global river  
820 channel network, *Earth interactions*, 2, 1-37, 1998.

821 Oki, T., Nishimura, T., and Dirmeyer, P. A.: Assessment of Annual Runoff from Land  
822 Surface Models Using Total Runoff Integrating Pathways (TRIP), *J Meteorol*, 77, 235-255,  
823 1999.

824 Peña-Arancibia, J., Van Dijk, A. I. J. M., Mulligan, M., and Renzullo, L. J.: Evaluation of  
825 precipitation estimation accuracy in reanalyses, satellite products and an ensemble method for  
826 regions in Australia and in south and east Asia, *Journal of Hydrometeorology*, accepted 29  
827 January 2013, 2013.

828 Pulliainen, J.: Mapping of snow water equivalent and snow depth in boreal and sub-arctic  
829 zones by assimilating space-borne microwave radiometer data and ground-based  
830 observations, *Remote Sensing of Environment*, 101, 257-269, doi: 10.1016/j.rse.2006.01.002,  
831 2006.

832 Rodell, M., Houser, P., Jambor, U., Gottschalck, J., Mitchell, K., Meng, C., Arsenault, K.,  
833 Cosgrove, B., Radakovich, J., and Bosilovich, M.: The global land data assimilation system,  
834 Bulletin American Meteorological Society, 85, 381-394, 2004.

835 Rui, H.: README Document for Global Land Data Assimilation System Version 1  
836 (GLDAS-1) Products, NASA, 2011.

837 Sakumura, C., Bettadpur, S., and Bruinsma, S.: Ensemble prediction and intercomparison  
838 analysis of GRACE time-variable gravity field models, Geophysical Research Letters, 41,  
839 1389-1397, 10.1002/2013GL058632, 2014.

840 Scipal, K., Holmes, T., de Jeu, R., Naeimi, V., and Wagner, W.: A possible solution for the  
841 problem of estimating the error structure of global soil moisture data sets, Geophysical  
842 Research Letters, 35, 2009.

843 Sheffield, J., Goteti, G., and Wood, E. F.: Development of a 50-year high-resolution global  
844 dataset of meteorological forcings for land surface modeling, Journal of Climate, 19, 3088-  
845 3111, 2006.

846 Sheffield, J., Wood, E. F., and Roderick, M. L.: Little change in global drought over the past  
847 60 years, Nature, 491, 435-438, 2012.

848 Stoffelen, A.: Toward the true near-surface wind speed: Error modeling and calibration using  
849 triple collocation, Journal of Geophysical Research: Oceans, 103, 7755-7766,  
850 10.1029/97jc03180, 1998.

851 Swenson, S., and Wahr, J.: Post-processing removal of correlated errors in GRACE data,  
852 Geophys. Res. Lett., 33, L08402, 10.1029/2005gl025285, 2006.

853 Swenson, S., Famiglietti, J., Basara, J., and Wahr, J.: Estimating profile soil moisture and  
854 groundwater variations using GRACE and Oklahoma Mesonet soil moisture data, Water  
855 Resour. Res., 44, W01413, 10.1029/2007wr006057, 2008.

856 Takala, M., Pulliainen, J., Metsamaki, S. J., and Koskinen, J. T.: Detection of Snowmelt  
857 Using Spaceborne Microwave Radiometer Data in Eurasia From 1979 to 2007, Geoscience  
858 and Remote Sensing, IEEE Transactions on, 47, 2996-3007, 10.1109/TGRS.2009.2018442,  
859 2009.

860 Tapley, B. D., Bettadpur, S., Ries, J. C., Thompson, P. F., and Watkins, M. M.: GRACE  
861 Measurements of Mass Variability in the Earth System, Science, 305, 503-505,  
862 10.1126/science.1099192, 2004.

863 Tregoning, P., McClusky, S., van Dijk, A., Crosbie, R. S., and Peña-Arancibia, J. L.:  
864 Assessment of GRACE satellites for groundwater estimation in Australia, National Water  
865 Commission, Caberra, 82, 2012.

866 van Dijk, A. I. J. M., and Renzullo, L. J.: Water resource monitoring systems and the role of  
867 satellite observations, *Hydrology and Earth System Sciences*, 15, 39-55, 10.5194/hess-15-39-  
868 2011, 2011.

869 van Dijk, A. I. J. M., Renzullo, L. J., and Rodell, M.: Use of Gravity Recovery and Climate  
870 Experiment terrestrial water storage retrievals to evaluate model estimates by the Australian  
871 water resources assessment system, *Water Resources Research*, 47, W11524.,  
872 10.1029/2011WR010714, 2011.

873 Van Dijk, A. I. J. M., Peña-Arancibia, J. L., Wood, E. F., Sheffield, J., and Beck, H. E.:  
874 Global analysis of seasonal streamflow predictability using an ensemble prediction system  
875 and observations from 6192 small catchments worldwide, *Water Resources Research*, DOI:  
876 10.1002/wrcr.20251, 10.1002/wrcr.20251, 2013.

877 Vörösmarty, C. J., and Moore III, B. I.: Modeling basin-scale hydrology in support of  
878 physical climate and global biogeochemical studies: An example using the Zambezi River,  
879 *Surveys in Geophysics*, 12, 271-311, 10.1007/bf01903422, 1991.

880 Wada, Y., van Beek, L. P. H., van Kempen, C. M., Reckman, J. W. T. M., Vasak, S., and  
881 Bierkens, M. F. P.: Global depletion of groundwater resources, *Geophysical Research*  
882 *Letters*, 37, L20402, 10.1029/2010gl044571, 2010.

883 Wada, Y., van Beek, L. P. H., Sperna Weiland, F. C., Chao, B. F., Wu, Y.-H., and Bierkens,  
884 M. F. P.: Past and future contribution of global groundwater depletion to sea-level rise,  
885 *Geophysical Research Letters*, 39, L09402, 10.1029/2012GL051230, 2012.

886 Wada, Y., Van Beek, R., Wanders, N., and Bierkens, M. F. P.: Human water consumption  
887 intensifies hydrological drought worldwide, *Environmental Research Letters*, 8, 034036,  
888 2013.

889 Wahr, J., Swenson, S., and Velicogna, I.: Accuracy of GRACE mass estimates, *Geophysical*  
890 *Research Letters*, 33, L06401, 10.1029/2005GL025305, 2006.

891 Wang, X., de Linage, C., Famiglietti, J., and Zender, C. S.: Gravity Recovery and Climate  
892 Experiment (GRACE) detection of water storage changes in the Three Gorges Reservoir of  
893 China and comparison with in situ measurements, *Water Resources Research*, 47, 2011.

894 Zaitchik, B. F., Rodell, M., and Reichle, R. H.: Assimilation of GRACE Terrestrial Water  
895 Storage Data into a Land Surface Model: Results for the Mississippi River Basin, Journal of  
896 Hydrometeorology, 9, 535-548, doi:10.1175/2007JHM951.1, 2008.

897 Zwieback, S., Scipal, K., Dorigo, W., and Wagner, W.: Structural and statistical properties of  
898 the collocation technique for error characterization, Nonlinear Processes in Geophysics, 19,  
899 69-80, 2012.

900

901

902 Table 1. Description and sources of data used in this analysis. Acronyms are explained in the  
 903 text.

Description	Source	Data access
<i>Prior estimates</i>		
model estimates (CLM, MOS, NOAA, VIC)	GLDAS	<a href="ftp://hydro1.sci.gsfc.nasa.gov/data/s4pa/GLDAS_V1/">ftp://hydro1.sci.gsfc.nasa.gov/data/s4pa/GLDAS_V1/</a> (data accessed 17 April 2013).
Model estimates (W3RA)		available from author Van Dijk
groundwater depletion		available from author Wada
river flow direction	TRIP	<a href="http://hydro.iis.u-tokyo.ac.jp/~taikan/TRIPDATA/Data/trip05.asc">http://hydro.iis.u-tokyo.ac.jp/~taikan/TRIPDATA/Data/trip05.asc</a> (downloaded 10 May 2013)
discharge from small catchments		available from author Van Dijk
discharge from large basins		<a href="http://www.cgd.ucar.edu/cas/catalog/surface/dai-runoff/index.html">http://www.cgd.ucar.edu/cas/catalog/surface/dai-runoff/index.html</a>
surface water extraction		available from author Wada
lake water level	Crop Explorer	<a href="http://www.pecad.fas.usda.gov/cropeplorer/global_reservoir/">http://www.pecad.fas.usda.gov/cropeplorer/global_reservoir/</a> (downloaded 9 May 2013)
new dam impoundments	Grand	<a href="http://atlas.gwsp.org/">http://atlas.gwsp.org/</a> (accessed 14 May 2014)
new dam impoundments	ICOLD	<a href="http://www.icold-cigb.org/">http://www.icold-cigb.org/</a> (accessed 14 May 2014)
sea level	AVISO	<a href="http://www.aviso.oceanobs.com/en/data/products/sea-surface-height-products/global/">http://www.aviso.oceanobs.com/en/data/products/sea-surface-height-products/global/</a> (downloaded 7 November 2013)
glacier extent	GGHYDRO	<a href="http://people.trentu.ca/~gcogley/glaciology/">http://people.trentu.ca/~gcogley/glaciology/</a> (downloaded 12 June 2013)
<i>Assimilated data</i>		
TWS: CSR, GFZ, JPL	Tellus	<a href="ftp://podaac-ftp.jpl.nasa.gov/allData/tellus/L3/land_mass/RL05/netcdf/">ftp://podaac-ftp.jpl.nasa.gov/allData/tellus/L3/land_mass/RL05/netcdf/</a> (downloaded 16 April 2013)
TWS: GRGS	CNES	<a href="http://grgs.obs-mip.fr/grace/variable-models-grace-lageos/grace-solutions-release-02">http://grgs.obs-mip.fr/grace/variable-models-grace-lageos/grace-solutions-release-02</a> (downloaded 16 April 2013)
glacial isostatic adjustment	Tellus	<a href="ftp://podaac-ftp.jpl.nasa.gov/allData/tellus/L3/land_mass/RL05/netcdf/">ftp://podaac-ftp.jpl.nasa.gov/allData/tellus/L3/land_mass/RL05/netcdf/</a> (downloaded 16 April 2013)
<i>Evaluation data</i>		
water level in large rivers	LEGOS HYDROWEB	<a href="http://www.legos.obs-mip.fr/en/soa/hydrologie/hydroweb/">http://www.legos.obs-mip.fr/en/soa/hydrologie/hydroweb/</a> (downloaded 13 October 2013)
<i>idem</i>	ESA River&Lake	<a href="http://tethys.eaprs.cse.dmu.ac.uk/RiverLake/shared/main">http://tethys.eaprs.cse.dmu.ac.uk/RiverLake/shared/main</a> (downloaded 25 October 2012)
snow depth	GLOBSNOW	<a href="http://www.globsnow.info/swe/archive_v1.3/">http://www.globsnow.info/swe/archive_v1.3/</a> (downloaded 9 October 2013)

905 Table 2. Spatial mean values (non-glaciated land areas only) of the error in monthly mass  
 906 change estimates for different GRACE and model sources as derived through triple  
 907 collocation. Also listed is the number of triple collocation estimates derived ( $N$ ) and the  
 908 spatial mean of the coefficient of variation (C.V.) in these  $N$  estimates.

	Mean error	Mean C.V.	N
	mm	%	
<i>GRACE</i>			
GRG	14.3	15	15
CSR	12.8	15	5
GFZ	15.5	11	5
JPL	15.2	12	5
Merged	13.5	–	–
<i>Models</i>			
CLM	26.7	6	3
MOS	21.9	7	3
NOAH	16.6	9	3
VIC	27.7	6	3
W3RA	17.9	7	3
Merged	18.1	–	–

909

910



911 Table 3. Calculated linear trends in global mean seasonally-adjusted anomalies associated  
 912 with different water cycle components for 2003–2012. The posterior trend estimates are also  
 913 expressed in equivalent sea level rise (SLR) and volume. Second number is standard  
 914 deviation.

Store	Prior	Posterior		
	global mean	global mean	SLR	Volume
	mm y <sup>-1</sup>	mm y <sup>-1</sup>	mm y <sup>-1</sup>	km <sup>3</sup> y <sup>-1</sup>
Sub-surface	-0.572 ± 0.029	0.017 ± 0.023	0.024 ± 0.032	9 ± 12
Rivers	0.012 ± 0.009	0.003 ± 0.01	0.004 ± 0.014	1 ± 5
Lakes	-0.012 ± 0.005	-0.021 ± 0.005	-0.029 ± 0.006	-11 ± 2
New dams	0.043 ± 0.001	0.032 ± 0.002	0.045 ± 0.003	16 ± 1
Seasonal snow	-0.022 ± 0.007	-0.035 ± 0.007	-0.049 ± 0.01	-18 ± 4
Arctic glaciers (>55°N)	0.265 ± 0.004	-0.604 ± 0.009	-0.849 ± 0.013	-308 ± 5
Antarctic glaciers (>55°S)	-	-0.301 ± 0.007	-0.423 ± 0.01	-154 ± 4
Remaining glaciers	-0.029 ± 0.004	-0.061 ± 0.003	-0.086 ± 0.004	-31 ± 2
Total terrestrial	-	-0.97 ± 0.035	-1.364 ± 0.049	-495 ± 18
Oceans	1.309 ± 0.044	1.029 ± 0.039	1.446 ± 0.054	525 ± 20

915

916

917

918 Table 4. Evaluation of alternative estimates of mean basin discharge using observations  
919 collated by Dai et al. (2009). Listed is the agreement for the ensemble models (without bias  
920 correction), the merged prior estimate and the posterior estimates resulting from reanalysis.

	CLM	MOS	NOAH	VIC	W3RA	prior	posterior
Combined discharge (km <sup>3</sup> y <sup>-1</sup> )	21,874	9,003	11,474	13,666	16,518	18,663	20,149
Diff. total (%)	5	-57	-45	-35	-21	-11	-4
RMSE (km <sup>3</sup> y <sup>-1</sup> )	114	184	126	147	63	47	44
Median  %  diff.	60	63	57	48	61	40	41

921

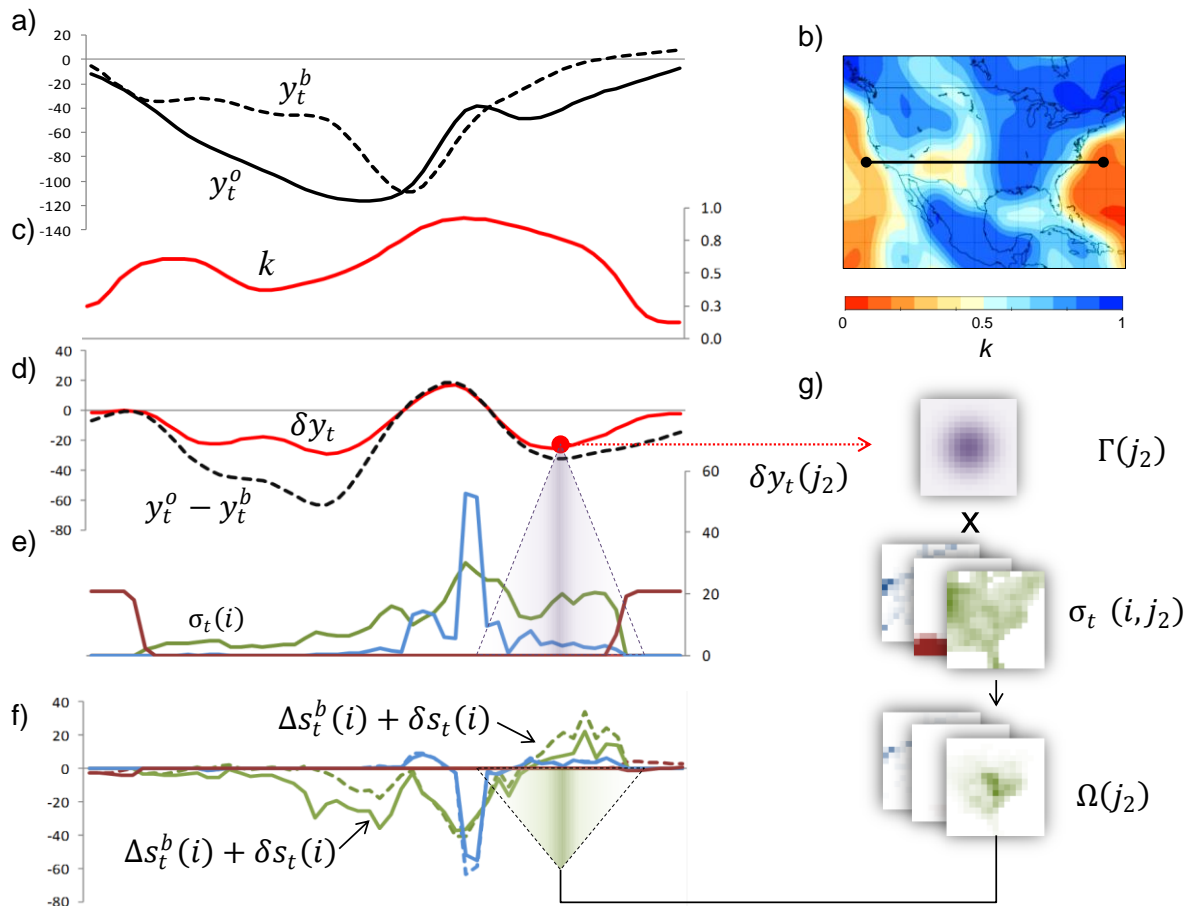
922

923

924 Table 5. Published trends in glacier water storage (Gardner et al., 2013; Jacob et al., 2012)  
 925 compared to estimates from reanalysis. Uncertainties are given at the 95% (2 standard  
 926 deviation) interval, superscripts refer to estimates derived from GRACE (g) or independent  
 927 methods (i). Also listed are regional trends attributed to other parts of the hydrological cycle,  
 928 and the ratio of the relative magnitude of that residual trends over estimated glacier mass  
 929 change.

Region	Reported	This study		
	trend (Gt y <sup>-1</sup> )	glacier trend (Gt y <sup>-1</sup> )	other components (Gt y <sup>-1</sup> )	ratio (%)
Greenland ice sheet + PGICs	-222 ± 9 <sup>g</sup>	-203 ± 10	-5 ± 1	3
Canadian Arctic Archipelago	-60 ± 6 <sup>i,g</sup>	-48 ± 3	-19 ± 2	39
Alaska	-50 ± 17 <sup>i,g</sup>	-23 ± 6	-23 ± 6	101
Northwest America excl. Alaska	-14 ± 3 <sup>i</sup>	3 ± 3	-8 ± 9	275
Iceland	-10 ± 2 <sup>i,g</sup>	-6 ± 1	-0.6 ± 0.2	10
Svalbard	-5 ± 2 <sup>i,g</sup>	-2 ± 1	0.1 ± 0.1	3
Scandinavia	-2 ± 0 <sup>i</sup>	0.4 ± 1.0	5 ± 2	>500
Russian Arctic	-11 ± 4 <sup>i,g</sup>	-4 ± 1	2 ± 2	47
High Mountain Asia	-26 ± 12 <sup>i,g</sup>	-29 ± 4	-15 ± 11	51
South America excl. Patagonia	-4 ± 1 <sup>i</sup>	-2 ± 1	-21 ± 33	>500
Patagonia	-29 ± 10 <sup>g</sup>	-15 ± 1	1 ± 2	4
Antarctica ice sheet + PGICs	-165 ± 72 <sup>g</sup>	-139 ± 8	0	0
Rest of world	-4 ± 0	-3 ± 1	82 ± 107	>500
Total	-549 ± 57	-471 ± 25		

930



931

932

933

934

935

936

937

938

939

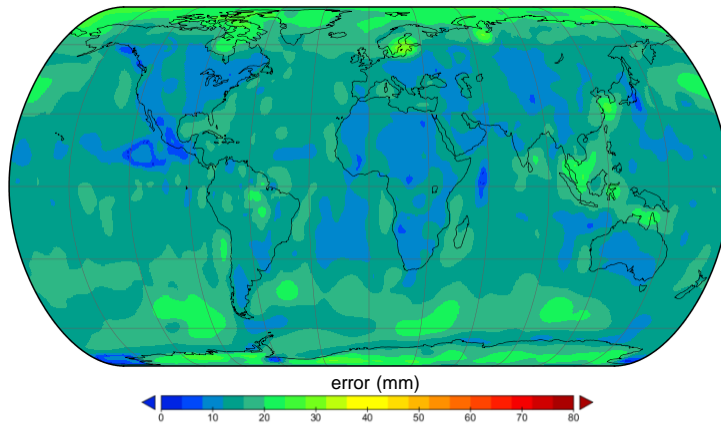
940

941

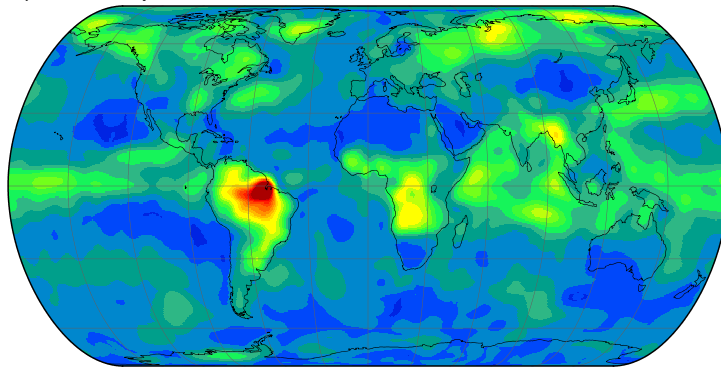
942

Figure 1. Illustration of the data assimilation approach followed using data along a transect through the USA for August 2003. Shown are: a) monthly satellite-derived TWS,  $y_t^o$ , and the equivalent prior estimate,  $y_t^b$ ; b) location of the West-East transect on a map of the gain matrix,  $k$ ; c) profile of  $k$  along the transect (cf. Figure 2c); d) calculation of the TWS analysis increment,  $\delta y_t$ , from  $k$  and innovation,  $(y_t^o - y_t^b)$ ; e) the prior error in the change of each of the stores,  $\sigma_t(i)$ ; f) the prior and posterior estimate of change in each store,  $\Delta s_t^b(i)$  and  $\Delta s_t^b(i) + \delta s_t(i)$ , resp.; and g) visual illustration of the disaggregation of the TWS analysis increments to the different stores. All units are in mm unless indicated otherwise; see text for full explanation of symbols; stores shown include the sub-surface (green), rivers (blue) and sea (dark red; remaining stores not shown for clarity).

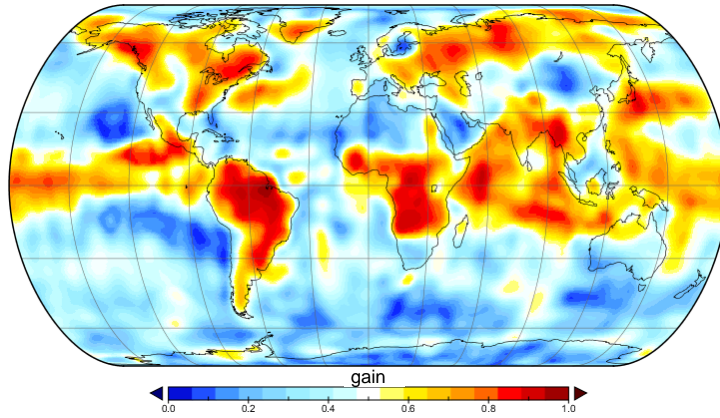
a) Error in GRACE



b) Error in prior



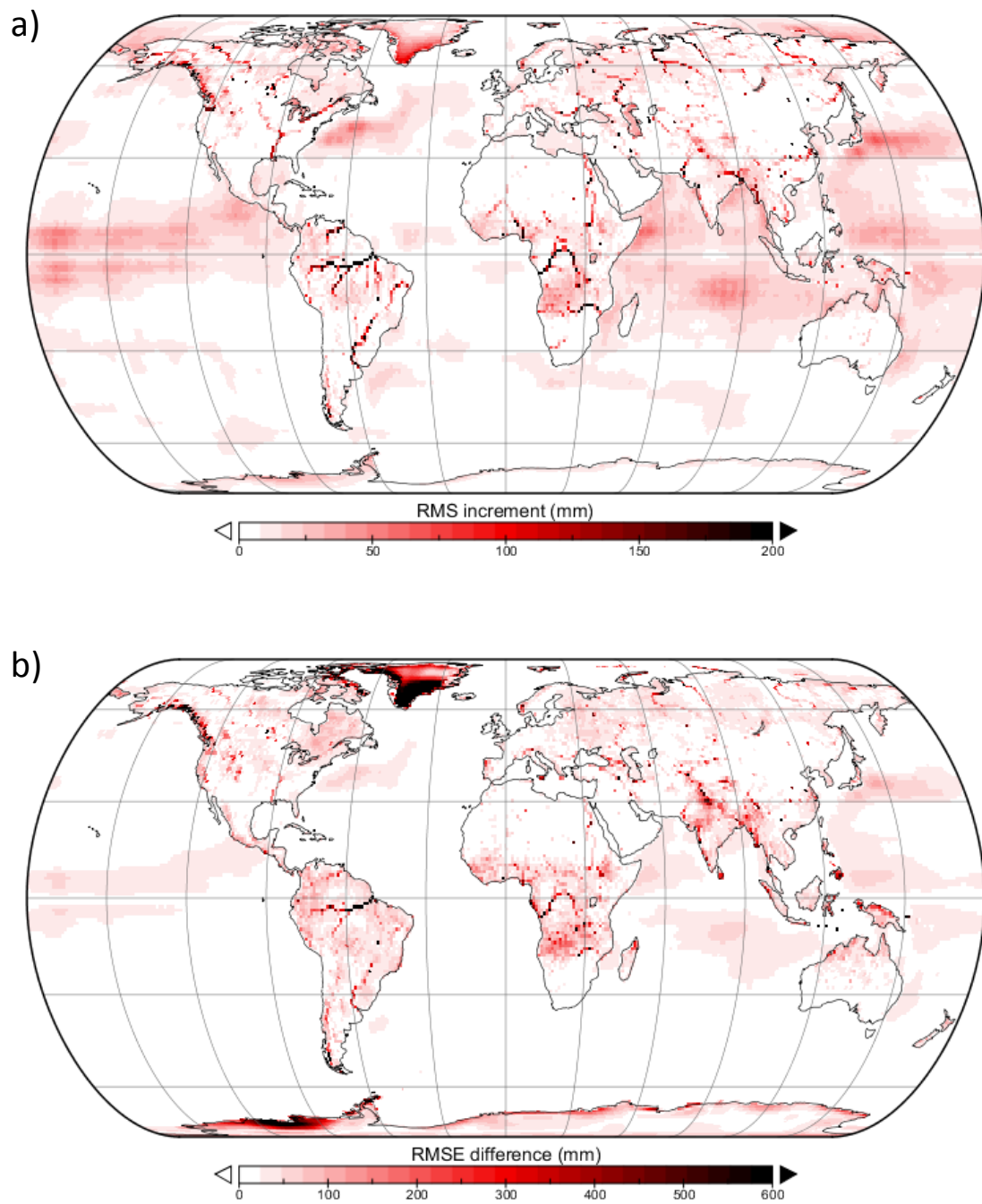
c) Gain



943

944 Figure 2. Triple collocation estimated error in storage change from the merged (a) GRACE  
945 and (b) prior estimates, and (c) resulting gain matrix.

946

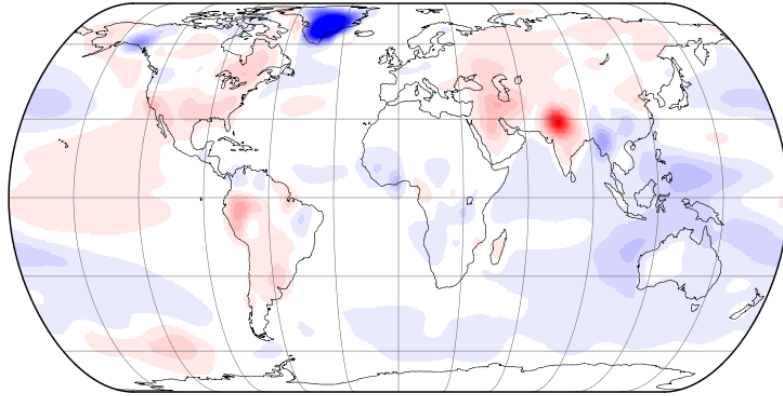


947

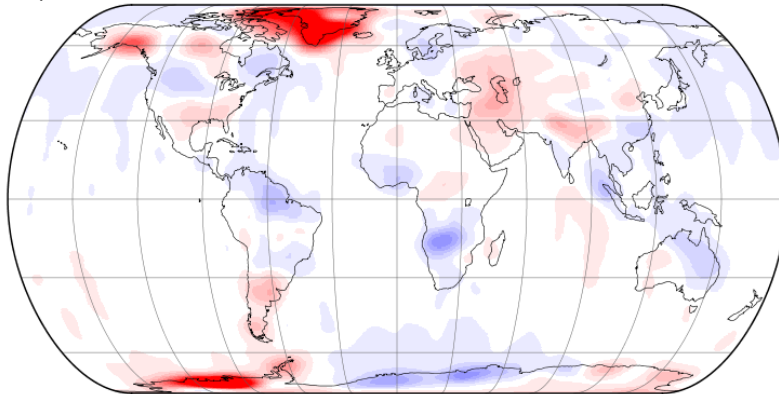
948 Figure 3. The impact of GRACE data assimilation on total water storage expressed as (a) the  
949 root mean square (RMS) analysis increment and (b) the RMS difference between prior and  
950 posterior storage time series.

951

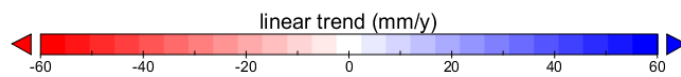
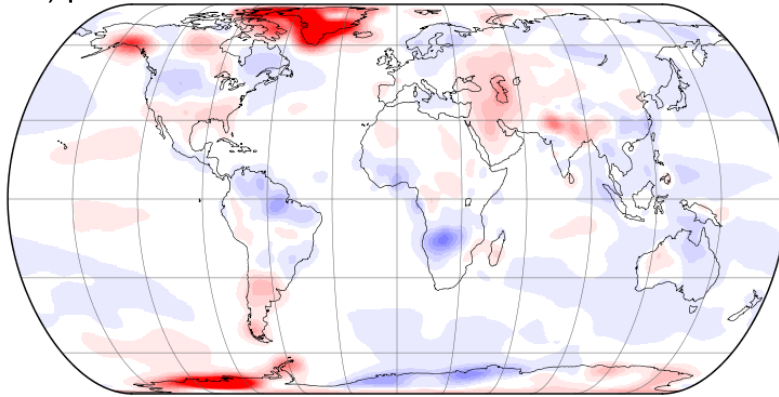
a) prior



b) GRACE



c) posterior

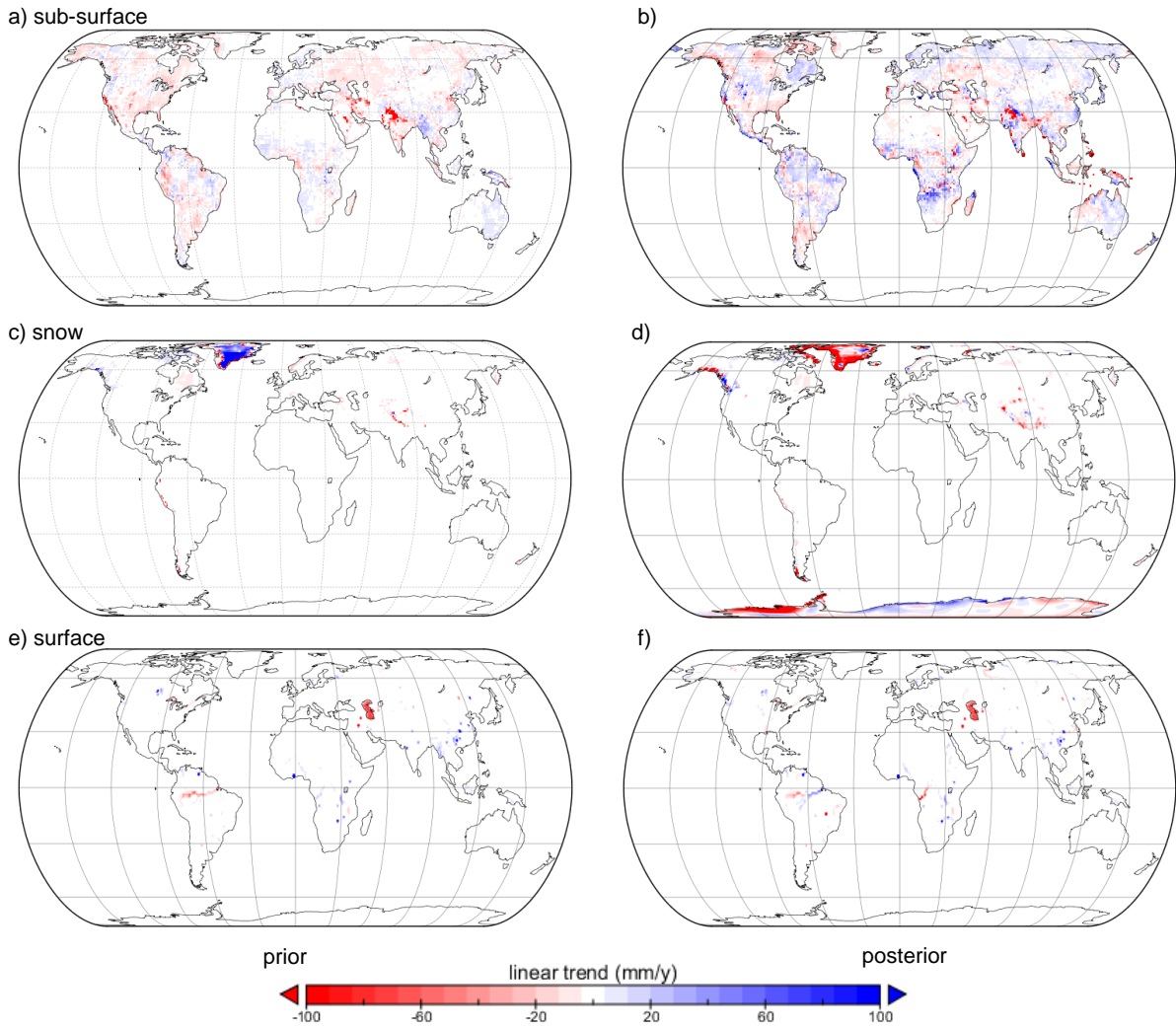


952

953 Figure 4. Trends in GRACE total water storage as derived from (a) prior storage estimates;

954 (b) merged satellite retrievals; and (c) posterior estimates.

955

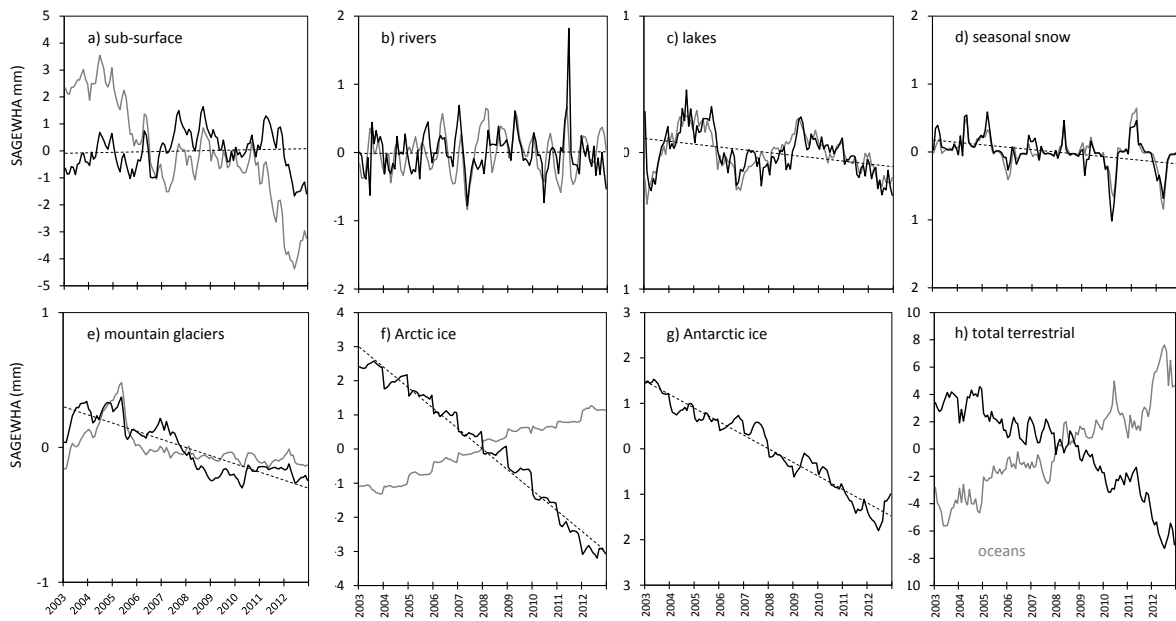


956

957 Figure 5. Trends in seasonal anomalies of prior (left column) and posterior (right column)  
 958 estimates of (a-b) sub-surface, (c-d) snow and (e-f) surface water (i.e., lake and river) water  
 959 storage.

960



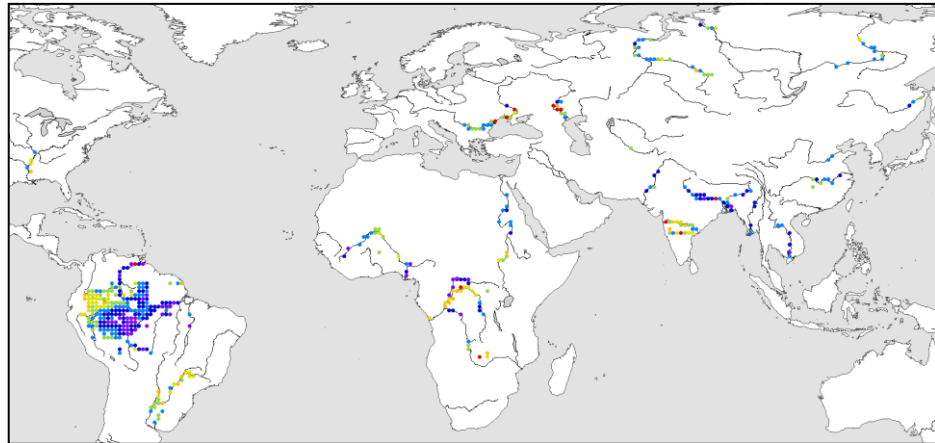
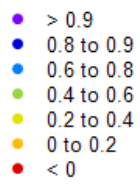


962

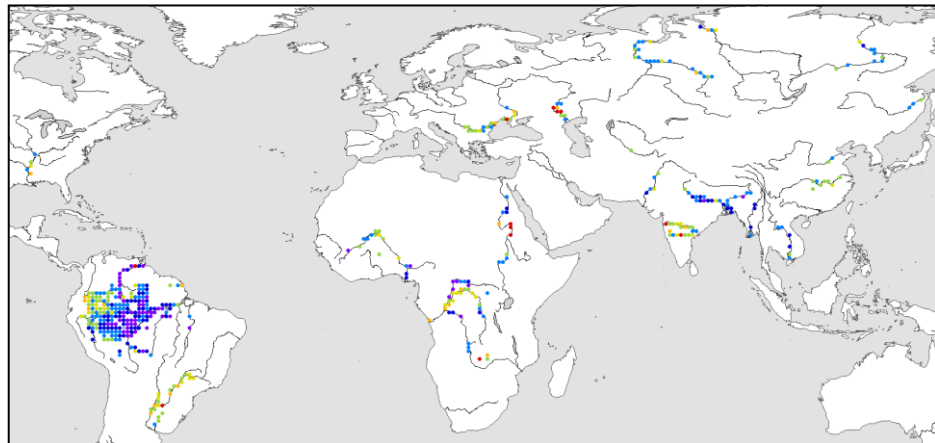
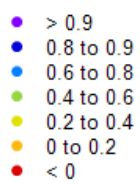
963 Figure 6. Time series of the prior (grey lines) and posterior (black lines) estimates of global  
 964 average seasonally-adjusted storage anomalies in different water cycle components. Dashed  
 965 lines show linear trends for 2003–2012 as listed in Table 3.

966

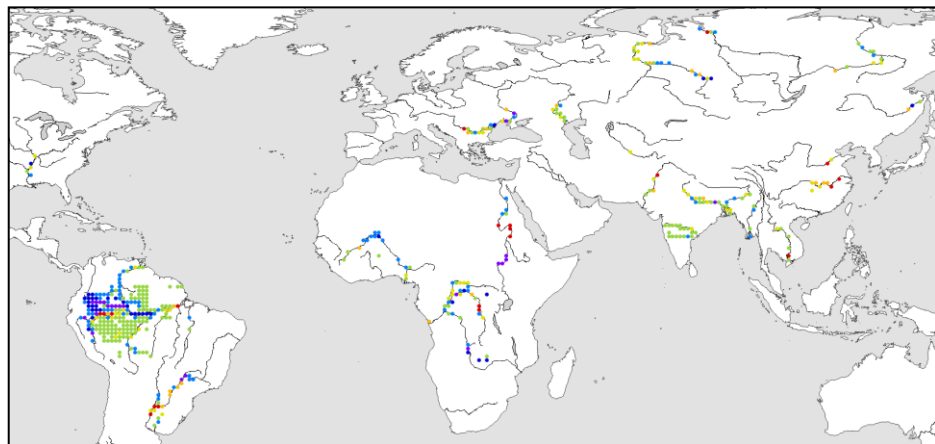
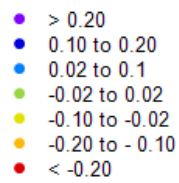
a) prior



b) posterior



c) change



967

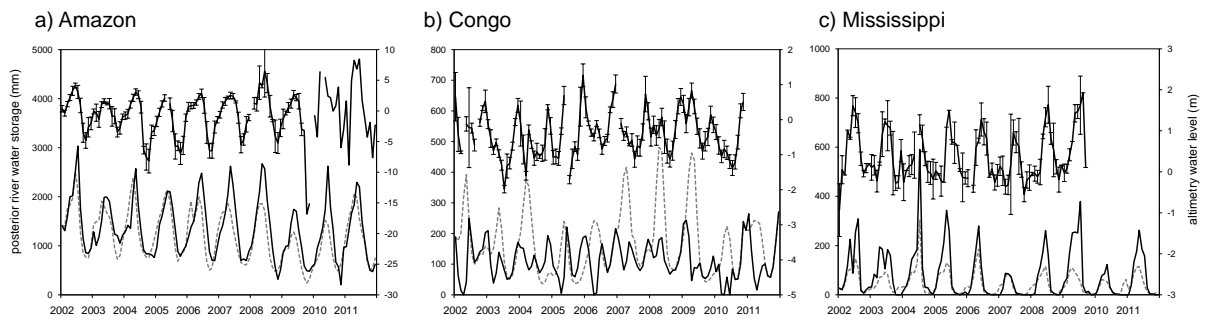
968 Figure 7. Effect of assimilation agreement with satellite altimetry river water levels:

969 Spearman's rank correlation coefficient ( $\rho$ ) for (a) prior and (b) posterior estimates and (c)

970 difference between the two.

971

972



973

974

Figure 8. Effect of assimilation agreement with satellite altimetry river water levels for grid

975

cells including the a) Amazon River ( $\sim 2.5^{\circ}\text{S}$ ,  $65.5^{\circ}\text{W}$ ;  $\rho$  changed from 0.71 for prior to 0.80

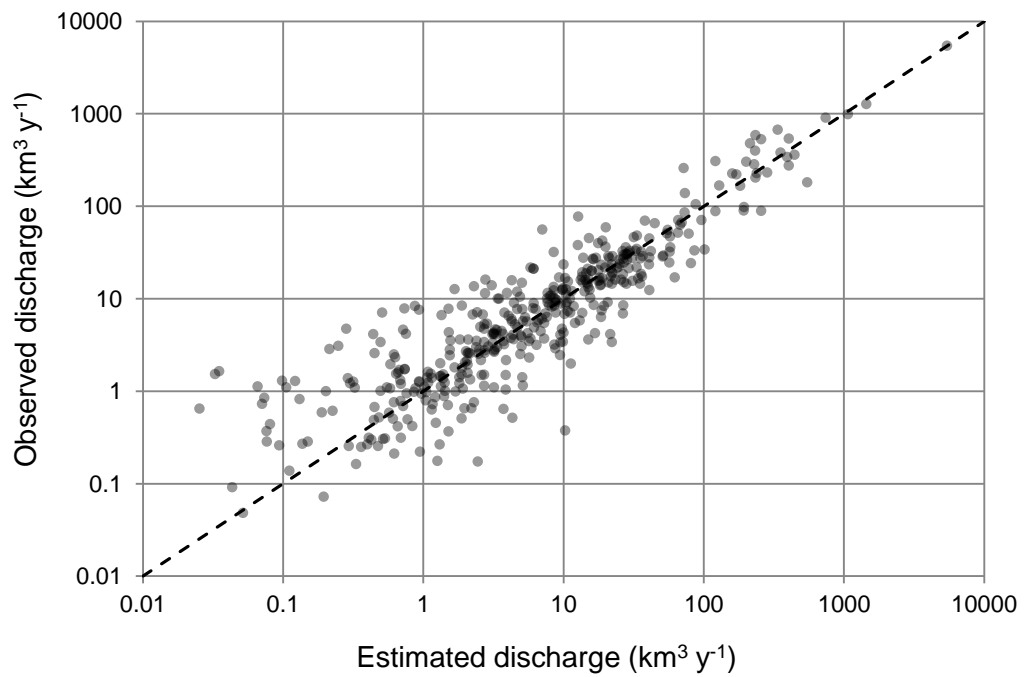
976

for posterior estimates); b) Congo River ( $\sim 2.5^{\circ}\text{N}$ ,  $21.5^{\circ}\text{E}$ ;  $\rho$  from 0.28 to 0.47) and

977

Mississippi River ( $35.5^{\circ}$ ,  $90.5^{\circ}\text{W}$ ;  $\rho$  from 0.37 to 0.56).

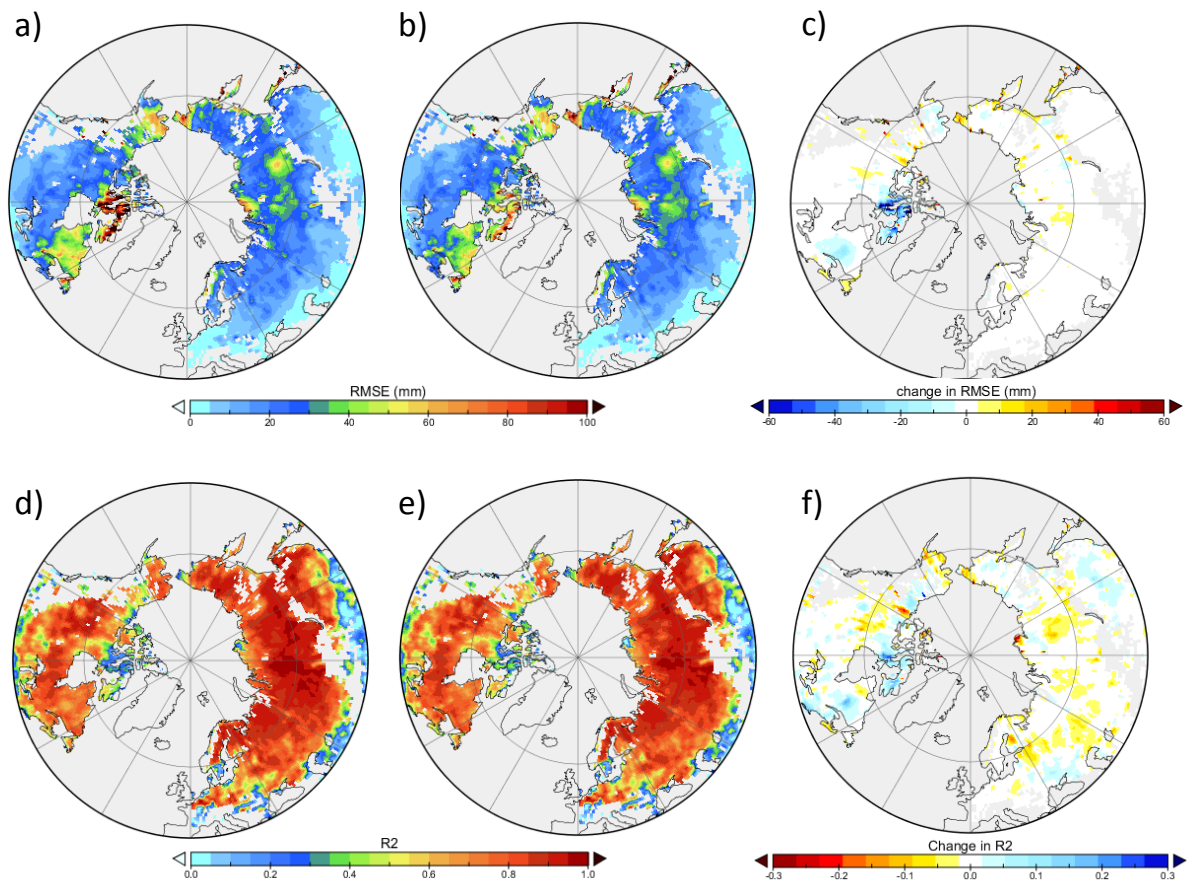
978



980

981 Figure 9. Comparison of mean basin discharge resulting from the analysis ( $Q_a$ ) and values  
982 based on observations (Dai et al., 2009) (darker areas indicate overlapping data points).

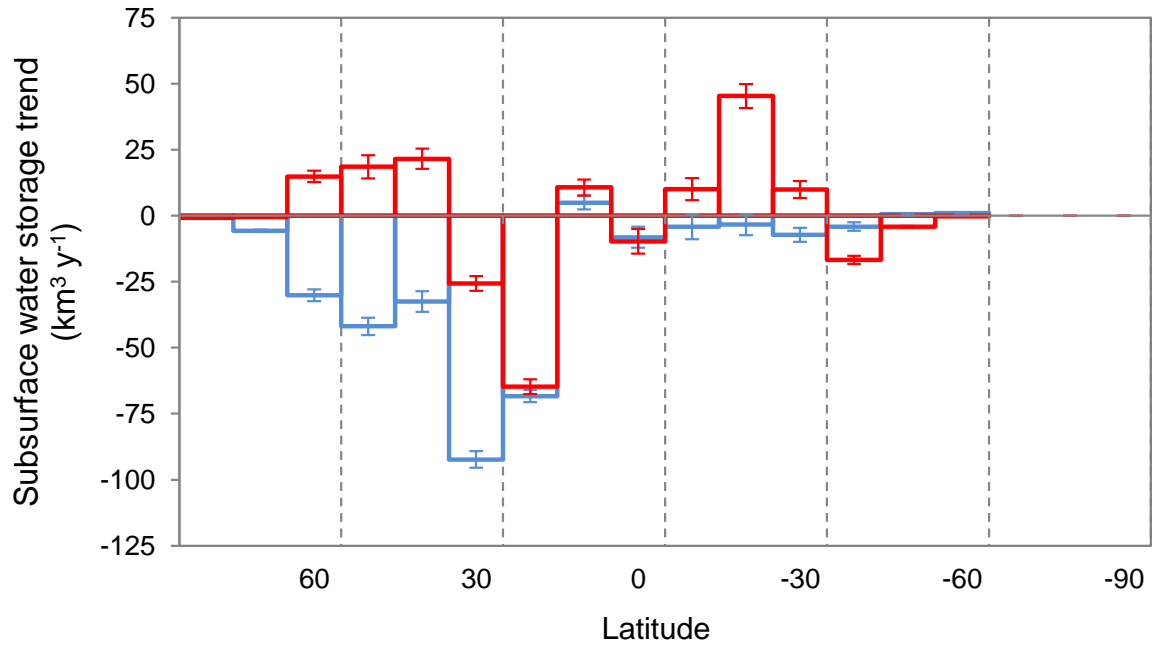
983



984

985 Figure 10. Effect of assimilation on agreement with GlobSnow snow water equivalent (SWE)  
 986 estimates, showing (a-c) root mean square error (RMSE) and (d-f) the coefficient of  
 987 correlation ( $R^2$ ). From left to right, agreement for (a,d) prior and (b, e) posterior estimates as  
 988 well as (c, f) the change in agreement.

989



990

991 Figure 11. Linear 2003–2012 trends in sub-surface water storage by 10° latitude band,  
 992 showing prior (blue) and posterior (red) estimates.

993